Network structure and input integration in competing firing rate models for decision-making

Victor J. Barranca, Han Huang & Genji Kawakita

Journal of Computational Neuroscience

ISSN 0929-5313

J Comput Neurosci
DOI 10.1007/s10827-018-0708-6

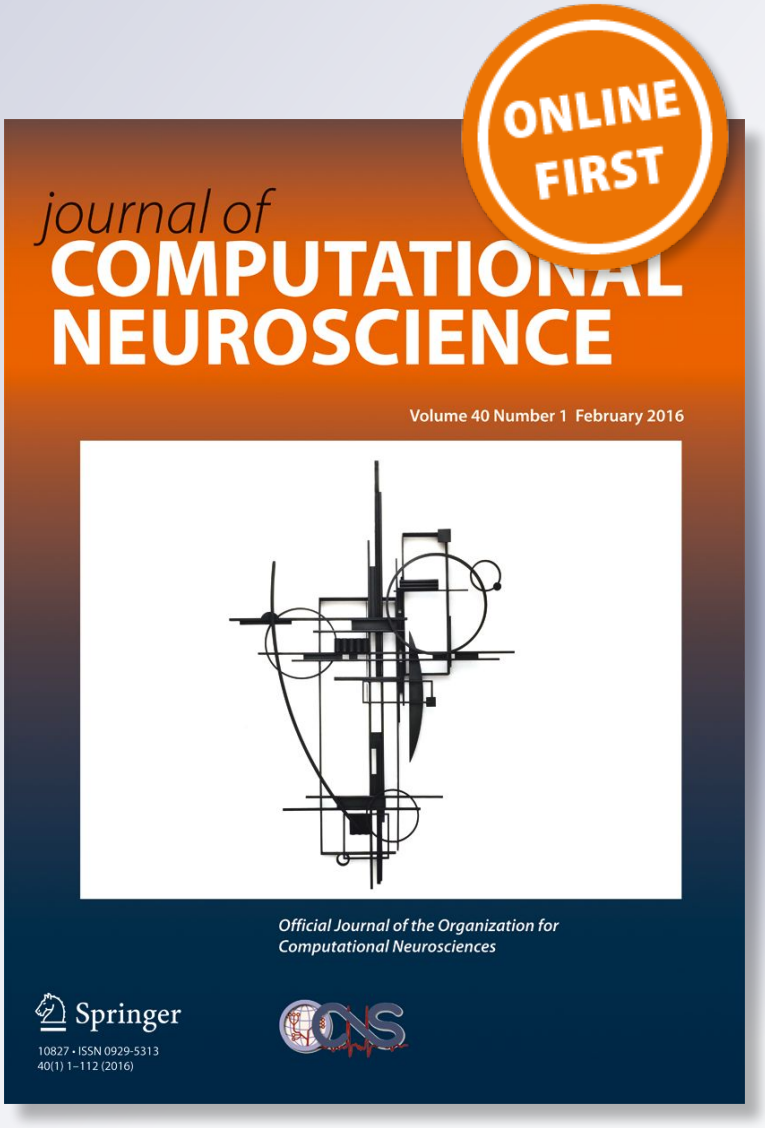

Springer

Journal of Computational Neuroscience
https://doi.org/10.1007/s10827-018-0708-6

Network structure and input integration in competing firing rate models for decision-making

Victor J. Barranca[1] · **Han Huang**[1] · **Genji Kawakita**[1]

Received: 19 October 2018 / Revised: 5 December 2018 / Accepted: 17 December 2018

Abstract

Making a decision among numerous alternatives is a pervasive and central undertaking encountered by mammals in natural settings. While decision making for two-option tasks has been studied extensively both experimentally and theoretically, characterizing decision making in the face of a large set of alternatives remains challenging. We explore this issue by formulating a scalable mechanistic network model for decision making and analyzing the dynamics evoked given various potential network structures. In the case of a fully-connected network, we provide an analytical characterization of the model fixed points and their stability with respect to winner-take-all behavior for fair tasks. We compare several means of input integration, demonstrating a more gradual sigmoidal transfer function is likely evolutionarily advantageous relative to binary gain commonly utilized in engineered systems. We show via asymptotic analysis and numerical simulation that sigmoidal transfer functions with smaller steepness yield faster response times but depreciation in accuracy. However, in the presence of noise or degradation of connections, a sigmoidal transfer function garners significantly more robust and accurate decision-making dynamics. For fair tasks and sigmoidal gain, our model network also exhibits a stable parameter regime that produces high accuracy and persists across tasks with diverse numbers of alternatives and difficulties, satisfying physiological energetic constraints. In the case of more sparse and structured network topologies, including random, regular, and small-world connectivity, we show the high-accuracy parameter regime persists for biologically realistic connection densities. Our work shows how neural system architecture is potentially optimal in making economic, reliable, and advantageous decisions across tasks.

Keywords Network structure · Firing rate models · Nonlinear dynamics · Decision-Making · Input integration

1 Introduction

Decision-making is central to the survival of a broad spectrum of species and, as a result, the ability to make an optimal selection among several alternatives is a skill that is likely fine-tuned through evolution. Everyday choices are typically made quickly and robustly upon integrating a small amount of information even in the presence of distractions and many possible alternatives. Despite its ubiquity, the underlying mechanism of choice in even the simplest settings remains to be fully characterized. Thus, decision making is now a central and interdisciplinary area of psychological, neurophysiological, and theoretical investigation.

Neurobiological experiments over the last several decades have demonstrated that several key areas of the brain, such as the prefrontal cortex, thalamus, basal ganglia, and parietal cortex, play an important role in decision-making tasks (Munakata et al. 2011; Platt and Glimcher 1999; Ding and Gold 2013). Activity in the awake monkey lateral intraparietal cortex area (LIP), for example, is highly correlated with simple visual motion discrimination tasks and displays particularly heightened activity around the time of a decision (Shadlen and Newsome 2001; Gold

Action Editor: David Terman

✉ Victor J. Barranca
vbarran1@swarthmore.edu

[1] Swarthmore College, 500 College Avenue, Swarthmore, PA 19081, USA

Published online: 19 January 2019

and Shadlen 2002). Similarly, the pre-motor cortex as well as dorsolateral prefrontal cortex contain pools of neurons that display gradually increased activity as perceptual information from upstream cortical layers is integrated, and the signature of this activity is highly correlated with specific choices (Schall 2001; Heekeren et al. 2008; de Lafuente and Romo 2006).

These physiological considerations suggest that when specific groups of neurons, commonly known as integrator neurons, display sufficiently high activity, a decision is made. This decision-making mechanism is the basis for several classes of mathematical models in which a particular choice is selected when one of several competing neuronal clusters exhibits a sufficiently high firing rate in response to upstream input. For instance, in the classical drift-diffusion model, one of two alternatives is to be selected as a noisy process integrates information akin to a random walk with drift, and when one of two decision boundaries is reached, a specific decision is made. A particular decision boundary can be interpreted to correspond to one group of neurons reaching a specific level of activity necessary to initiate a choice, and the model well reflects experimental data for a wide array of psychological tasks (Ratcliff 1978; Ratcliff et al. 2016). The modeling methodology, however, is not straightforward to generalize to tasks with a larger number of alternatives, as independent racing single-boundary diffusion processes lack the response competition inherent in the classical two-alternative forced choice framework. The leaky competing accumulator (LCA) model instead facilitates the competition of an arbitrary number of neuronal assemblies by directly including lateral inhibition between all clusters (Usher and McClelland 2001).

While the LCA model is capable of reflecting more alternatives through the inclusion of additional nodes and corresponding differential equations, the input into a particular node may become arbitrarily high, especially as the number of alternatives becomes large. Additionally, the standard LCA model assumes that neuronal clusters integrate information linearly over time. While there is experimental evidence suggesting a linear input-output mapping in certain operating regimes (Ahmed et al. 1998; Mason and Larkman 1990), a sigmoidal transfer function is more physiological, broadly valid, and potentially yields more gradual integration of evidence (Dayan and Abbott 2001; Hodgkin and Huxley 1952; Polsky et al. 2004; Marreiros et al. 2008; Rauch et al. 2003; Miller and Katz 2013).

In this work, we formulate a scalable mechanistic network model framework for decision making and analyze the model performance in the context of several network structures as well as alternative means of input integration, demonstrating agreement with physiological constraints and prevalent experimental observations. We utilize an attractor-based system in which each attractor corresponds to a specific choice. An attractor such that the output of a particular node, which in this case reflects the firing activity of a pool of neurons, is significantly more active than the remaining nodes displays winner-take-all (WTA) behavior. Systems demonstrating WTA dynamics are able to display important computational characteristics beyond decision making, such as selective amplification, state-dependent processing, sequence learning, classification, and signal restoration (Rutishauser et al. 2011; McKinstry et al. 2016; Luo et al. 2017; Krizhevsky et al. 2017), with important applications in machine learning and artificial intelligence (You and Wang 2017). Though typical attractor models require fine-tuning of parameters such that stable WTA dynamics are garnered (Binas et al. 2014), our model demonstrates accurate WTA dynamics for a stable set of parameters largely invariant with respect to the number of alternatives and task difficulty.

The dynamical properties associated with attractor-based decision-making models with idealized structure have been the subject of intense mathematical investigation, yielding an extensive characterization of the uniqueness and stability of attractors capable of gleaning accurate decision-making dynamics. Nevertheless, the majority of previous theoretical studies were limited to classical models with fully-connected network structure or non-physiological integration of inputs (Ermentrout 1992; Rutishauser et al. 2011; Maass 2000; Fukai and Tanaka 1997; Mao and Massaquoi 2007). There is a great deal of evidence suggesting the connectivity between neuronal clusters is relatively sparse and not entirely random (Perin et al. 2011; Markram et al. 1997; Mason et al. 1991; He et al. 2007), and thus we also address the dynamics of our attractor model in the context of several network structures beyond fully dense connectivity. While recent analysis of detailed physiological models has given important insights into the neural circuitry of inhibitory control, receptor function, and decision stopping (Wang 2002; Wei and Wang 2016), we instead focus on fundamental mechanisms impacting decision-making dynamics, such as input gain and network structure, in the context of a minimal yet physiologically motivated network model.

We first introduce our competing firing rate network model and its biological motivation in Section 2. We develop a theoretical framework for measuring key decision-making properties, including accuracy, response time, and task difficulty, and discuss how these measures

relate to task alternatives and integration of inputs. In Section 3.1, we proceed by analyzing the decision-making dynamics of our model in the case of a fully-connected network, particularly for several gain functions with varying steepness. Given analytical methods are more amenable in this context, we analyze the existence, uniqueness, and stability of winner-take-all fixed points given sigmoidal and then binary gain functions in Sections 3.1.1 and 3.1.2, respectively.

Investigating the impact of input integration on network dynamics, we show in Section 3.2 that for fair decision-making tasks, our model with sigmoidal gain yields an optimal parameter regime which is largely invariant with respect to the number of alternatives and difficulty of tasks. Crucially, optimal accuracy is achieved for lateral inhibition strengths that satisfy intuitive energetic constraints on decision making. Later, we demonstrate in Section 3.3, via asymptotic analysis and numerical simulation, that as sigmoidal gain becomes steep, akin to a binary transfer function, more accurate decision making is achieved at the cost of increased response time. On the other hand, in Section 3.4, we show that sigmoidal input integration maintains significantly higher levels of accuracy in the presence of noise as well as connection removal. These results suggest that more gradual input integration was selected by evolution to facilitate swift and successful decision making over a broad spectrum of conditions. In Section 3.5, we analyze the model dynamics for random, regular, and small-world network structures, demonstrating the same optimal lateral inhibition strengths persist across network topologies over a broad range of connection densities. We further observe that the decision-making accuracy is closely tied to the network clustering properties, with maximal choice fidelity well corresponding to biologically realistic network structure. Finally, we discuss the implications and potential extensions of this work in Section 4.

2 Model and methods

To study the decision-making properties of neuronal clusters, we construct a competing firing rate network model with nonlinear dynamics. Firing rate models are canonically utilized to reflect the collective dynamics of a large number of neurons, and have emerged in the study of diverse phenomena, including content addressable memories, sleep-wake cycle dynamics, and perceptual bistability (Wilson and Cowan 1972; Hopfield 1982; Patel and Rangan 2017; Shpiro et al. 2007). Here we focus on the firing rate dynamics for neuronal clusters evoked in response to a task requiring a forced decision to be selected among multiple alternatives.

In our competing firing rate network model, the state of the ith node, $x_i(t)$, reflects the firing rate of the ith *neuronal assembly* at time t in response to incoming input from upstream layers and is governed by

$$\frac{dx_i}{dt} = -x_i + f\left(-\sum_{\substack{j=1\\ j\neq i}}^{N} \frac{w}{p(i)} A_{ij}x_j + S_i\right), \tag{1}$$

where there are N competing neuronal clusters, w is the lateral inhibition strength, S_i is the incoming evidence for the ith cluster, $p(i)$ is the incoming degree of the ith cluster, and $f(\cdot)$ is the *gain function* determining the integration of input. The recurrent connectivity among the nodes is prescribed by the $N \times N$ adjacency matrix $A = (A_{ij})$, which indicates the presence or absence of inhibition from the jth cluster to the ith cluster. We consider decision-making dynamics for *fair* tasks corresponding to initial conditions $x_i = I$ for $i = 1, \ldots, N$, such that all clusters begin with an identical firing rate $I > 0$. For concreteness, we assume the initial firing rate I and the incoming upstream inputs S_i are bounded in the unit interval $[0, 1]$.

It is important to note that by normalizing the connection strength for the ith node by its incoming degree $p(i)$, the expected recurrent input into a neuronal cluster is approximately invariant with respect to network size and node degree. Without such a normalization, as typical in alternative decision-making models, the recurrent input would potentially grow with the number of neuronal clusters, and thus the decision-making dynamical regime would be intricately impacted by the number of alternatives in a task. We will initially assume the network is fully-connected in Section 3.1 for analytical tractability and examine alternative sparser network structures later in Section 3.5.

While we will consider several choices of nonlinear gain functions, we assume in general that f is nondecreasing and bounded in $[0, 1]$ to reflect general physiological observations. These properties well agree with the lower and upper firing rate bounds for neuronal assemblies. Intuitively, an upper bound must exist due to neuronal refractory periods following firing events and a lower bound must exist since full quiescence corresponds to minimal activity. We analyze the effect of two particular classes of gain functions, namely sigmoidal and binary gain, on decision-making dynamics (Dayan and Abbott 2001; Hodgkin and

Huxley 1952; Polsky et al. 2004; Marreiros et al. 2008; Rauch et al. 2003). The sigmoidal gain function has form

$$f(x) = \frac{1}{1 + e^{-k(x-b)}}, \tag{2}$$

where k prescribes the steepness and b determines the center of $f(x)$. Note that $f(0)$ is positive and generally small, indicating that some neurons in the clusters will still fire at relatively low rates in the absence of external inputs, as observed in awake mammals (Yamada et al. 1989; Wilson and Cowan 1972; Rauch et al. 2003).

In the limit of infinitely large steepness, $k \to \infty$, the sigmoid approaches a binary gain function

$$f(x) = \begin{cases} 1, & x \geq b \\ 0, & x < b, \end{cases} \tag{3}$$

with center b. Unless specified otherwise, in our model simulations we choose $b = 0.5$, which is the expected firing rate for a node assuming each x_i is uniformly distributed on domain $[0, 1]$, and $k = 4$ for relatively gradual integration of $\mathcal{O}(1)$ inputs. For graphical comparison, the sigmoidal and binary gain functions are depicted in Fig. 1a.

In further contrasting our modeling framework from prior decision-making models, it is also necessary to emphasize that all inputs are integrated by a single gain function as typical in more physiological rate models. Alternative decision-making models instead typically assume that separate gain functions integrate each recurrent input. Reformulating our model framework into the context of separated gain yields

$$\frac{dx_i}{dt} = -x_i + \left[-\sum_{\substack{j=1 \\ j \neq i}}^{N} \frac{w}{p(i)} A_{ij} f(x_j) + S_i \right]^+, \tag{4}$$

where $[\cdot]^+$ is the positive part function, which guarantees nonnegative firing rates (Fukai and Tanaka 1997; Mao and Massaquoi 2007; Usher and McClelland 2001). However, the model given by Eq. (4) has several undesirable decision-making properties relative to the single gain function framework that we utilize in this work. For example, in the single gain function network model prescribed by Eq. (1), x_i remains bounded in $[0, 1]$ for initial conditions in this unit interval, whereas the separated gain function model in Eq. (4) is generally unbounded. The boundedness of Eq. (1) is guaranteed since $x_i' \geq 0$ when $x_i = 0$ and $x_i' \leq 0$ when $x_i = 1$, for $i = 1, \ldots, N$, yielding a compact region over which decision-making accuracy may be analyzed.

Comparing the two modeling frameworks further, it is significant to observe that in the large inhibition limit, the separated gain function model with sigmoidal integration approaches a fixed point such that all neuronal clusters are quiescent. This yields no means for the network to parse decision alternatives. Since f is non-decreasing, $f(0) > 0$, and $0 \leq S_i \leq 1$, the recurrent input into the ith node, $\sum_{j \neq i} \frac{w}{p(i)} A_{ij} f(x_j)$, is $\mathcal{O}(w)$, and is greater in magnitude than the upstream layer input S_i for sufficiently large w. Thus, large lateral inhibition evokes exponential decay to quiescence across all nodes and thereby no decision-making capability. In the single gain function setting, however, the cluster with the largest external input would still generally fire at the highest rate, showing a graded response important for winner-take-all dynamics. Considering that in both the resting-state and under external stimulation, cerebral circuits demonstrate a rich repertoire of active dynamical states, determined in part by the underlying network structure as well as the stream of ongoing cognitive inputs (Barttfeld et al. 2015; Deco et al. 2011), it is most informative to analyze model dynamics in which at least a single cluster of neurons is active.

With our modeling framework formulated, we now develop a natural means for defining the accuracy, response

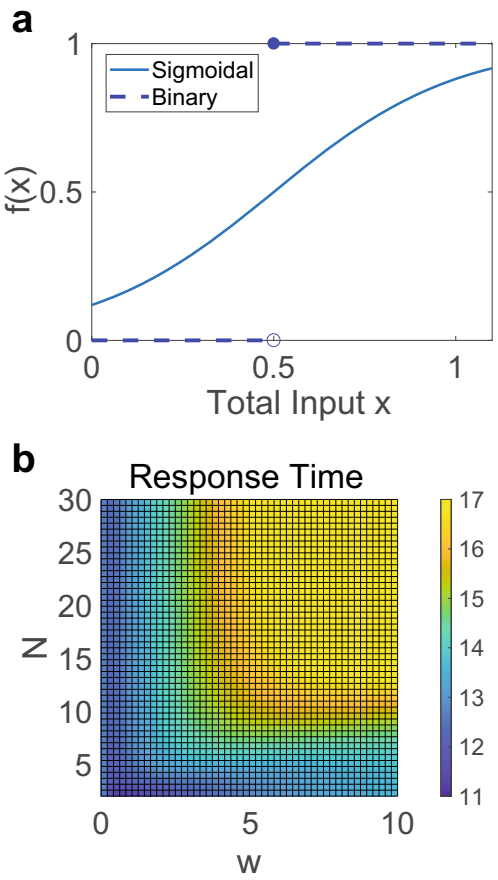

Fig. 1 Gain functions and Hick's law. a Sigmoidal (solid) and binary (dashed) gain function response $f(x)$ to a common set of inputs x. **b** Normalized response time as a function of the number of alternatives, N, and the lateral inhibition strength, w, for a fully-coupled network with sigmoidal gain and easy task difficulty. For relatively small N, we observe an approximately logarithmic growth in normalized response time with the number of alternatives, as suggested by Hick's law

time, and difficulty corresponding to a particular task. When the network reaches a fixed point, the neuronal clusters may be divided into two sets, namely the set of nodes, W, that achieve the maximal firing rate, x_w, and the set of all remaining nodes, L. If only a single neuronal assembly achieves a maximal firing rate at steady-state, the system demonstrates winner-take-all dynamics. In this case, the difference between the maximal firing rate and the second largest firing rate, $x_w - \max_{l \in L} x_l$, defines the decision *accuracy*. A task with high accuracy thus demonstrates large separation between the highest neuronal cluster firing rate and the remaining cluster firing rates, yielding a clear optimal choice.

Physiologically, the *response time* corresponds to the time transpired from the onset of a choice-related stimulus to the moment an action corresponding to a specific decision is initiated. In the context of our model, the response time is naturally interpreted as the time elapsed from the initial condition until stationary dynamics are achieved. Such decision making is analogous to free response tasks, where individuals make a decision over a time horizon of their own design. We compute the time elapsed until the system reaches a fixed point numerically by requiring that the magnitude of total change in the output of all clusters is sufficiently small over a given time horizon. Note that we observe numerically and show analytically over a broad parameter regime that the model is indeed guaranteed to reach a unique fixed point, and thus our methodology for determining accuracy and response time is robustly well defined. While Eq. (1) is a deterministic dynamical system, we also investigate how our analysis extends to a noisy system in Section 3.4. In the stochastic model, we utilize an analogous notion of accuracy based on the output of the clusters after sufficient time passes, corresponding to an interrogation task that requires a response after an alloted time period, since such a stochastic system never reaches a fully stationary state.

In the context of an experiment, the *difficulty* of a task is generally gauged by the closeness in the profitability of the various alternatives. In our model, task difficulty is determined by the distribution of incoming evidence, S_i, for $i = 1, \ldots, N$, and particularly the difference between the largest two inputs from the upstream layer. We thus define the decision difficulty as $1 - (\max_i S_i - \max_{j \neq i} S_j)$, which is bounded in the unit interval $[0, 1]$ and yields a value of unity for maximally challenging tasks such that at least two alternatives have identical profitability. A *simple* task is considered to be one for which there is only a single node with maximal evidence greater than the gain function center b, and for such tasks we typically observe the greatest decision-making fidelity across network structures. In our analysis, we generally consider three difficulties for concreteness, where one particular node receives maximal evidence $S_i = S_w$ and all other nodes receive evidence $S_j = S_l$ for $j \neq i$. In each case, maximal evidence $S_w = 1$, with (i) *easy* corresponding to $S_l = 0.2$, (ii) *medium* corresponding to $S_l = 0.5$, and (iii) *hard* corresponding to $S_l = 0.8$. The easy task is simple, whereas the medium and hard tasks are non-simple and demonstrate increasingly higher difficulty.

For relatively easy forced-decision tasks, it is generally found in experiments that as the number of alternatives increases, the response time for a fixed level of accuracy increases approximately logarithmically, thereby following Hick's law (Hick 1952). In our model framework, we verify Hick's law by gradually increasing the number of task alternatives and computing the corresponding model response time normalized by accuracy, so as to analogously demand an individual may take the necessary time to achieve a specified level of accuracy. For easy tasks, we see rapid growth in normalized response time given a small number of alternatives, which ultimately levels off for tasks with sufficiently numerous options. We plot, for example, in Fig. 1b the normalized response time dependence on the number of alternatives, N, and the lateral inhibition strength, w, for a fully-connected network and easy task difficulty. We note that across a broad range of inhibition strengths, Hick's law is well obeyed, with larger w generally yielding increased response times.

3 Results

3.1 All-to-all network analysis

Given its analytical tractability and conventional utilization in decision-making models, we first analyze a fully-connected, or all-to-all, network in the context of our model framework. In our analysis, it is important to note that for a fully-connected network the incoming degree of all nodes is identical with $p(i) = N - 1$ since each cluster receives inhibition from all other clusters. Assuming fair initial conditions such that $x_i = I$ for $i = 1, \ldots, N$ as well as evidences $S_i = S_w$ and $S_j = S_l$ for $j \neq i$, the network dynamics reduce to a planar system of two nonlinear differential equations. In particular, we need only investigate the firing rate dynamics of the cluster receiving maximal evidence, x_w, and dynamics of the remaining clusters, x_l, which are identical in this case since nodes in set L receive the same incoming evidence. Therefore, Eq. (1) reduces to

$$\frac{dx_w}{dt} = -x_w + f(-wx_l + S_w) \tag{5a}$$

$$\frac{dx_l}{dt} = -x_l + f\left(-wx_l - \frac{w}{N-1}(x_w - x_l) + S_l\right), \tag{5b}$$

for which analysis of fixed points and their stability, which determine decision-making accuracy, is tractable. A numerical investigation of the model accuracy as a function of the number of alternatives and lateral inhibition strength for each of the three difficulties and the two gain functions is depicted in Fig. 2. For each plot, the accuracy averaged over 100 fair initial conditions is depicted. In the case of the model with binary gain, we observe that for sufficiently large lateral inhibition, the network achieves nearly perfect accuracy. A downside, however, is that, particularly in more difficult cases, the necessary large inhibition between neuronal clusters is not physiological. Moreover, the optimal choice of large w is not stable across difficulties and numbers of alternatives, indicating a lack of robustness for binary integration of evidence. For sigmoidal gain, we instead observe a clear optimal span of relatively small inhibition strengths for which maximal accuracy is achieved, agreeing with energetic constraints on interactions between clusters, and the location of this extremum is preserved across the number of alternatives and difficulty associated with tasks. Hence, no fine-tuning of parameters is necessary in general. While the maximum accuracy achieved by the sigmoidal gain function is typically lower than that which is optimally achieved via binary gain, we will see in Sections 3.4 and 3.5 that networks with sigmoidal gain are significantly more robust to noise as well as deviations in network structure.

For a decision to be well resolved and an optimal alternative to be selected with nonzero probability, the model network must achieve a unique and asymptotically stable fixed point, such that the neuronal cluster with highest incoming evidence is most active. As expected intuitively, we generally see that as the difficulty of a task increases, the maximal accuracy, corresponding to the separation between the highest two firing rates at a fixed point, typically decreases. In providing an analytical characterization of these decision-making dynamics, we first consider a sigmoidal gain function in Section 3.1.1 and then similarly examine model dynamics in the context of a binary gain function in Section 3.1.2. In our initial theoretical analysis, we will focus on model fixed points and their stability across the number of alternatives and difficulty associated with a task. By demonstrating that the dynamical system model is guaranteed to approach a unique fixed point for a given set of parameter choices, we are able to robustly determine decision-making accuracy by comparing the output of neuronal assemblies upon reaching a steady-state. The theoretical results obtained for the all-to-all network thus provide a strong basis for subsequently interpreting the model dynamics in networks with more realistic topology. For the cases in which a unique asymptotically stable fixed point does not exist, by averaging accuracy over a large number of initial conditions, we are still able to compare decision-making dynamics across dynamical regimes.

3.1.1 Winner-take-all attractors given a sigmoidal gain function

Since Eq. (1) with sigmoidal gain is a continuous dynamical system on the compact and convex set $[0, 1]^N$, Brouwer's fixed point theorem guarantees the existence of a fixed point in $[0, 1]^N$ (Brouwer 1912). Note the existence of a fixed point is indeed assured across all network topologies and is not only limited to the all-to-all network considered in this section.

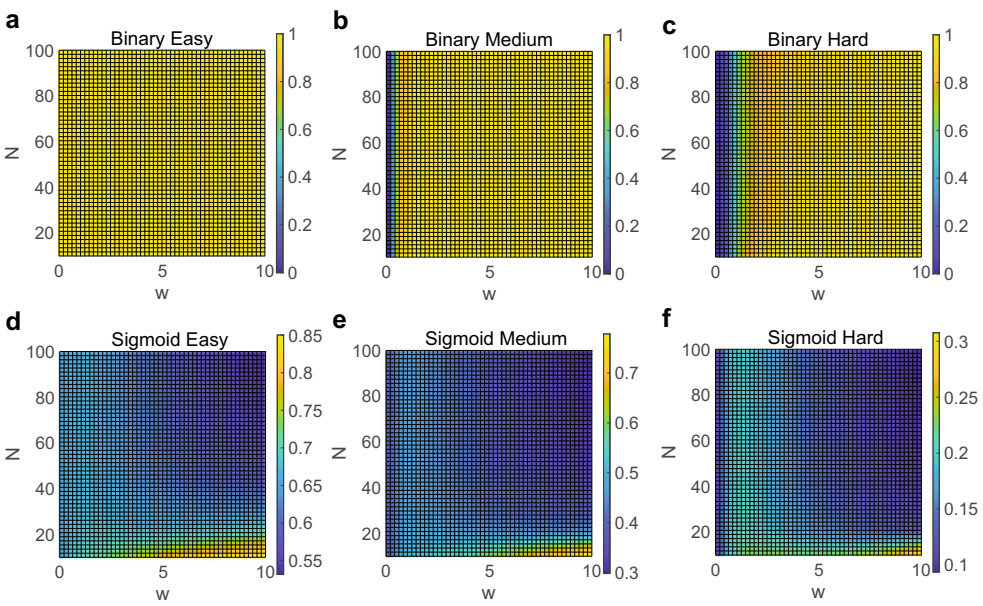

Fig. 2 Dynamics of all-to-all network. a–c Accuracy dependence on number of alternatives, N, and lateral inhibition strength, w, in the case of a binary gain function for easy, medium, and hard difficulties, respectively. **d–f** Accuracy dependence on number of alternatives, N, and lateral inhibition strength, w, in the case of a sigmoidal gain function for easy, medium, and hard difficulties, respectively. For each plot, the network is fully-connected and the accuracy computed via numerical simulation averaged over 100 fair initial conditions is depicted

The uniqueness of the fixed point is guaranteed for the fully-coupled network under conditions on both the lateral inhibition strength and steepness of the sigmoidal gain function, which are given below and demonstrated in the Appendix A.

Uniqueness of Fixed Point with Sigmoidal Gain: The decision-making network model given in Eq. (1) with sigmoidal gain function f as prescribed by Eq. (2) has a unique fixed point if there exists positive constant M such that $f'(x_i) \leq M, \forall x_i$, and $\frac{wM}{N-1} < 1$ for $i = 1, \ldots, N$.

The sufficient conditions shown for uniqueness of the fixed point require a balance between the maximal sigmoid slope, M, and the lateral inhibition strength, w, such that their product is less than unity. Thus, a steeper gain function requires smaller inhibition. In the context of sigmoidal gain functions demonstrating gradual integration of information, as depicted in Fig 1a, the restriction for uniqueness is automatically satisfied in the set of w that yield optimal decision accuracy. Note that while a similar property could be analogously proven for an alternative version of our model that does not incorporate normalization by incoming degree, stricter restrictions on w are generated as instead $wM < 1$ is required if normalization by $p(i)$ is omitted.

Since the dynamics of Eq. (1) are equivalent to the planar system (5) in our analysis, the Poincaré-Bendixon theorem guarantees the asymptotic stability of the unique fixed point (Bendixson 1901; Andronov 1973). Given the reduced model dynamics are confined to $[0, 1]^2$ and Bendixon's criterion rules out the existence of limit cycles, the system must approach the unique attractor after sufficiently long time elapses. We observe empirically that indeed the model demonstrates winner-take-all dynamics in approaching this attractor, yielding positive accuracy in Fig. 2d–f for a broad range of w and N.

3.1.2 Winner-take-all attractors given a binary gain function

In light of the discontinuity of the binary gain function prescribed by Eq. (3), we are required to use an alternate methodology to characterize the model network dynamics with binary gain.

For simple tasks such that $S_w > b$ and $S_l < b$ for $l \neq w$, the binary network model exhibits a unique asymptotically stable fixed point with perfect accuracy across all positive choices of w, N, and initial conditions, as indicated in Fig. 2 (a). In this case, the fixed point for all clusters receiving low evidence is $x_l^* = f(-\sum_{j \neq l} \frac{w}{N-1} A_{lj} x_j^* + S_l) \leq f(S_l) = 0$ since f is a binary function with center b. The fixed point for the node receiving maximal evidence is therefore $x_w^* = f(-\sum_{j \neq i} A_{ij} \frac{w}{N-1} x_j^* + S_w) = f(S_w) = 1$. Considering all clusters $i \neq w$ exhibit exponential decay in firing rate towards zero, this unique fixed point with perfect accuracy is asymptotically stable. Note this analysis makes no specific assumptions regarding the network topology,

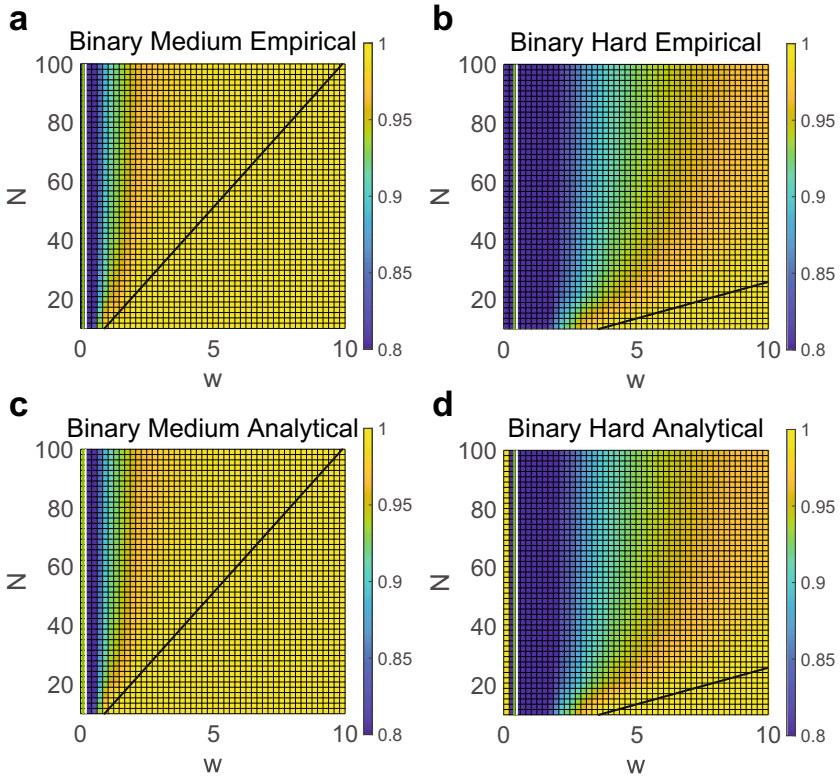

Fig. 3 Comparison of analytical and empirical accuracy for all-to-all networks with binary gain. a-b Numerically computed accuracy dependence on the number of alternatives, N, and lateral inhibition strength, w, in the case of a binary gain function for medium and hard difficulties, respectively, magnified in the high accuracy region by cutting off accuracies less than 0.8 for enhanced visual comparison. **c–d** Analogous plots using the analytically computed accuracy for medium and hard difficulties, respectively. The green line corresponds to the first part of assumption (7a), the black line corresponds to the second part of assumption (7a), and the white line corresponds to assumption (7b). Each network is fully-connected and, for each empirical plot, the accuracy averaged over 100 fair initial conditions is depicted

and thus applies across network connectivity, as verified empirically in Section 3.5.

For tasks that are non-simple, the previous result no longer applies, and the nature of the model dynamics is determined by the number of alternatives, lateral inhibition, and difficulty of the task. For fair tasks such that $w > (N-1)(S_l - b)$ and $N \geq 3$, there is a unique fixed point, $x_w^* = 1, x_l^* = 0$, for the reduced planar system (5). This is a natural consequence of eliminating the possibility of the three other potential fixed points with alternative combinations of x_w^* and x_l^* taking on binary values. We observe that this unique perfect accuracy fixed point requires a larger choice of lateral inhibition strength for tasks with more alternatives, which is not likely to be enacted physiologically since this would potentially require excessively large lateral inhibition. An analogous argument for the asymptotic stability of the fixed point as utilized in the case of the sigmoidal gain function may be applied using the generalization of Poincaré-Bendixon theory to dynamical systems with jump discontinuities, noting that for the large w required in the uniqueness of the fixed point, the divergence of Eq. (5) in the distributional sense is negative (Melin 2005). From Fig. 2**a**–**c**, it is empirically clear that the fixed point is asymptotically stable. A magnified version of these accuracy plots for tasks of medium and hard difficulty is depicted in Fig. 3**a** and **b**, showing perfect accuracy across all initial conditions in this parameter regime.

There is a large parameter regime over which $w \leq (N-1)(S_l - b)$ and consequently the fixed point analyzed previously no longer exists for non-simple tasks. In this case, we generally observe, from numerical simulation, that the network evolves towards an attracting state nearby which $x_w \to 1$ and x_l demonstrates extremely small oscillations that decay in magnitude with decreasing time-step size. While this attracting state is not a fixed point in the traditional sense since the system is not completely stationary, the oscillations about the attracting state, which we refer to as a *perturbed fixed point*, are infinitesimally small in the true dynamical system. Intuitively, the perturbed fixed point manifests when the input into the gain function for x_l hovers around threshold b. We summarize the dynamics about the perturbed fixed point in the property below, which we demonstrate in the Appendix B.

Global Attraction to the Perturbed Fixed Point with Binary Gain: For non-simple and fair tasks with number of alternatives $N \geq 3$, the reduced decision-making network model given in Eq. (5) with binary gain function f as prescribed by Eq. (3) is globally attracted to the perturbed fixed point such that

$$\lim_{t\to\infty} x_w = 1, \tag{6a}$$

$$\lim_{t\to\infty} x_l \in [z, z+\epsilon), \tag{6b}$$

for any $\epsilon > 0$ under assumptions

$$N > \max\left(\frac{2w-(S_l-b)}{w-(S_l-b)}, \frac{w}{S_l-b}+1\right), \tag{7a}$$

$$w > S_l - b, \tag{7b}$$

where

$$z = \frac{(N-1)(S_l-b)-w}{(N-2)w}. \tag{8}$$

We verify our analysis in the case of medium and hard difficulties empirically, and show strong agreement between the accuracy corresponding to the theoretical perturbed fixed point, $1-z$, and the accuracy determined via simulation. Comparing the accuracy computed analytically, depicted in Fig. 3c and d, to the numerically computed accuracy in Fig. 3a and b, we see the results are nearly indistinguishable over a broad range of parameters, w and N. The only noticeable deviation occurs when $w < S_l - b$, for which assumptions (7) and our theory do not apply. These dynamics together preclude the possibility of an optimal parameter regime for relatively small w in the case of binary gain, and thus the system is unable to achieve high accuracy via low lateral inhibition strength as observed using sigmoidal gain.

3.2 Optimal network parameters

As observed empirically in Section 3.1, the sigmoidal gain function facilitates an optimal span of relatively small lateral inhibition strengths for which maximal accuracy is achieved over tasks with varying numbers of alternatives and difficulty. We demonstrate the existence of such an optimal parameter regime in the limit of a large number of alternatives, $N \to \infty$, and further show that our approximation still holds well for finite and relatively small N. We consider the reduced system given by Eq. (5) in the large N limit, with fixed points reducing to $x_w^* = f(-wx_l^* + S_w)$ and $x_l^* = \lim_{N\to\infty} f\left(-\frac{(N-2)}{N-1}wx_l^* - \frac{w}{N-1}x_w^* + S_l\right) = f(-wx_l^* + S_l)$. We solve the resultant transcendental system of equations for the approximate fixed point numerically for large N and a range of w. In particular, in Fig. 4, we compare the accuracy determined via the fixed point approximation with the accuracy computed through numerical simulation. The numerical and approximate accuracies are nearly identical, yielding the highest accuracy for a similar range of small lateral inhibition strengths in each case. We see that the ideal span of w in the large N limit agrees well with the optimal inhibition strengths identified for a small number of alternatives in Fig. 2d–f. While the peak accuracy achieved using sigmoidal gain is still lower than the maximal accuracy computed via binary gain, the small magnitude and stability

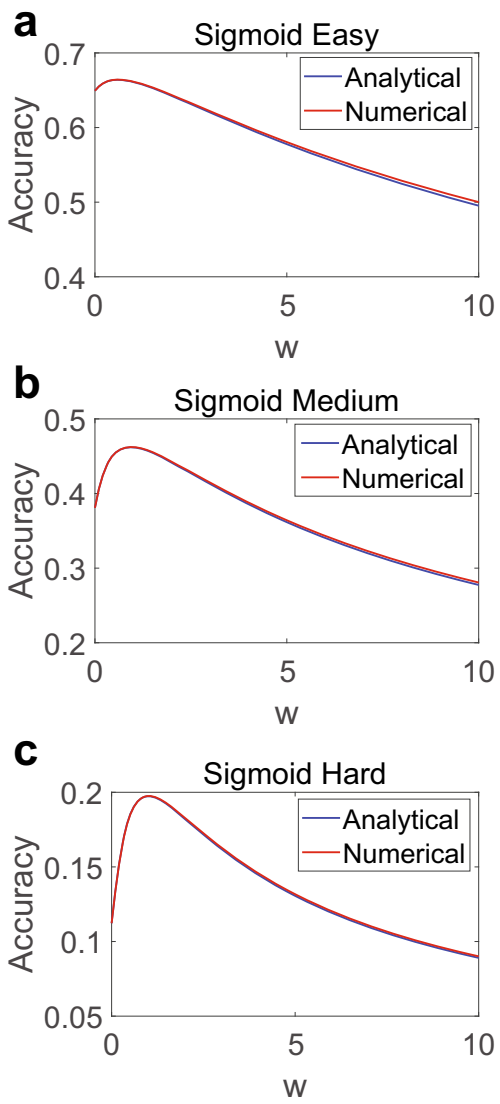

Fig. 4 Accuracy in the limit of a large number of alternatives for all-to-all networks with sigmoidal gain. a–c Accuracy dependence on lateral inhibition strength, w, in the case of a sigmoidal gain function in the large number of alternatives limit for easy, medium, and hard difficulties, respectively. In each case, the accuracy computed using the large N approximation is depicted in blue and the accuracy computed via numerical simulation is plotted in red. Each network is fully-connected with $N = 100$ and, for each empirical plot, the accuracy averaged over 100 fair initial conditions is depicted

of the optimal lateral inhibition strengths make sigmoidal integration of evidence suited for a wider spectrum of tasks and efficient in requiring relatively low energy expenditure via weak interaction between neuronal clusters.

3.3 Impact of gain function steepness

In comparing the two classes of gain functions, it is significant to observe that in the large steepness limit, $k \to \infty$, sigmoidal integration approaches binary gain. For this reason, we utilize asymptotic analysis to demonstrate the impact of sigmoid steepness on decision-making accuracy. We later numerically investigate the effect on response time in the context of our model framework.

We determine a two-term asymptotic expansion for the fixed point of reduced model (5) assuming sigmoidal gain of high steepness. In doing so, the leading order term of the expansion yields the fixed point corresponding to binary gain, whereas the second term takes into account the effects of finite steepness, from which we can approximate the impact of sigmoidal steepness on accuracy. Note that we make identical assumptions as given in Eq. (7) when determining the perturbed fixed point for the network model with binary gain. Letting steepness $k = \frac{1}{\epsilon}$ for $0 < \epsilon \ll 1$ in Eq. (2) yields small parameter ϵ in which we will expand the transcendental system of equations determining the model fixed point

$$x_w^* = f(-wx_l^* + S_w) \tag{9a}$$

$$x_l^* = f(-Ax_l^* - Bf(-wx_l^* + S_w) + S_l), \tag{9b}$$

where $A = w\frac{N-2}{N-1}$ and $B = \frac{w}{N-1}$ for notational convenience. Note Eq. (9b) is rewritten in terms of x_l^* only, and thus we determine the expansion for x_l^* first and later use it to determine the expansion for x_w^*.

Before expanding with respect to x_l^*, we rewrite Eq. (9b) explicitly in terms of the sigmoidal gain function

$$\frac{1}{1+e^{\epsilon^{-1}\left(Ax_l^* + \frac{B}{1+e^{\epsilon^{-1}(wx_l^*+b-S_w)}} + b - S_l\right)}} = x_l^*,$$

and then rearrange terms so as to determine the impact of small parameter ϵ in our analysis, yielding

$$-Ax_l^* - \frac{B}{1+e^{\epsilon^{-1}(wx_l^*+b-S_w)}} - b + S_l = \epsilon \ln\left(\frac{x_l^*}{1-x_l^*}\right).$$

We assume asymptotic expansion $x_l^* \sim x_0 + \mu(\epsilon)x_1 + \ldots$ and thus obtain

$$\begin{aligned} &- A(x_0+\mu(\epsilon)x_1+\ldots) - \frac{B}{1+e^{\epsilon^{-1}(w(x_0+\mu(\epsilon)x_1+\ldots)+b-S_w)}} \\ &- b + S_l = \epsilon \ln\left(\frac{x_0+\mu(\epsilon)x_1+\ldots}{1-(x_0+\mu(\epsilon)x_1+\ldots)}\right). \end{aligned} \tag{10}$$

Letting $\epsilon \to 0$ yields the leading $\mathcal{O}(1)$ equation

$$-Ax_0 - \frac{B}{1+e^{\epsilon^{-1}(w(x_0)+b-S_w)}} - b + S_l = 0,$$

and leading order term $x_0 = \frac{(N-1)(S_l-b)-w}{(N-2)w} = z$, agreeing with the perturbed fixed point for the model with binary gain given by Eq. (8).

Next, we determine the finite-steepness correction term, $\mu(\epsilon)x_1$, in the asymptotic expansion. Expanding Eq. (10) in geometric series, we obtain

$$\begin{aligned} &-A(x_0+\mu(\epsilon)x_1+\dots)-b+S_l \\ &-B\left(1-e^{\epsilon^{-1}w(x_0+\mu(\epsilon)x_1+\dots)+b-S_w}+\dots\right) \\ &=\epsilon\ln\left(\frac{x_0+\mu(\epsilon)x_1+\dots}{1-(x_0+\mu(\epsilon)x_1+\dots)}\right) \end{aligned}$$

Proceeding in the asymptotic hierarchy requires gauge function $\mu(\epsilon)=\epsilon$. Equating $\mathcal{O}(\epsilon)$ terms, we obtain

$$-Ax_1=\ln\left(\frac{x_0+\epsilon x_1+\dots}{1-(x_0+\epsilon x_1+\dots)}\right),$$

yielding $x_1=\ln\left(\frac{1-z}{z}\right)/A$. Hence, the two-term asymptotic expansion for x_l^* is

$$x_l^*\sim z+\epsilon\frac{N-1}{(N-2)w}\ln\left(\frac{1-z}{z}\right)+\dots \tag{11}$$

and may be utilized in Eq. (9a) to generate the two-term expansion for x_w^*. Assuming $x_w^*\sim x_0'+\mu'(\epsilon)x_1'+\dots$, it follows

$$\begin{aligned} x_0'+\mu'(\epsilon)x_1'+\dots&=\frac{1}{1+e^{\epsilon^{-1}\left(w\left(z+\epsilon\frac{\ln\left(\frac{1-z}{z}\right)}{A}+\dots\right)+b-S_w\right)}} \\ &=1-e^{\epsilon^{-1}\left(w\left(z+\epsilon\frac{\ln\left(\frac{1-z}{z}\right)}{A}+\dots\right)+b-S_w\right)}+\dots, \end{aligned}$$

and matching terms in the asymptotic hierarchy yields $x_0'=1$, $\mu'(\epsilon)=e^{-\epsilon^{-1}(S_w-wz-b)}$, and $x_1'=-e^{\frac{N-1}{N-2}\ln\left(\frac{1-z}{z}\right)}$. Thus, the two-term asymptotic expansion for x_w^* is

$$x_w^*\sim 1-e^{-\frac{1}{\epsilon}(S_w-wz-b)}e^{\frac{N-1}{N-2}\ln\left(\frac{1-z}{z}\right)}+\dots \tag{12}$$

Before interpreting the asymptotic expansion with respect to decision-making accuracy, we note that our analysis yields a high fidelity approximation for the model fixed points, particularly for sigmoidal steepness $k>10$. In Fig. 5 (a)-(b), we depict the relative error in the approximation using the difference in accuracy computed via the two-term asymptotic expansion and numerical simulation for tasks of medium and hard difficulty. We see that only for especially small w, which violate assumptions (7), does the approximation yield error that is not negligible.

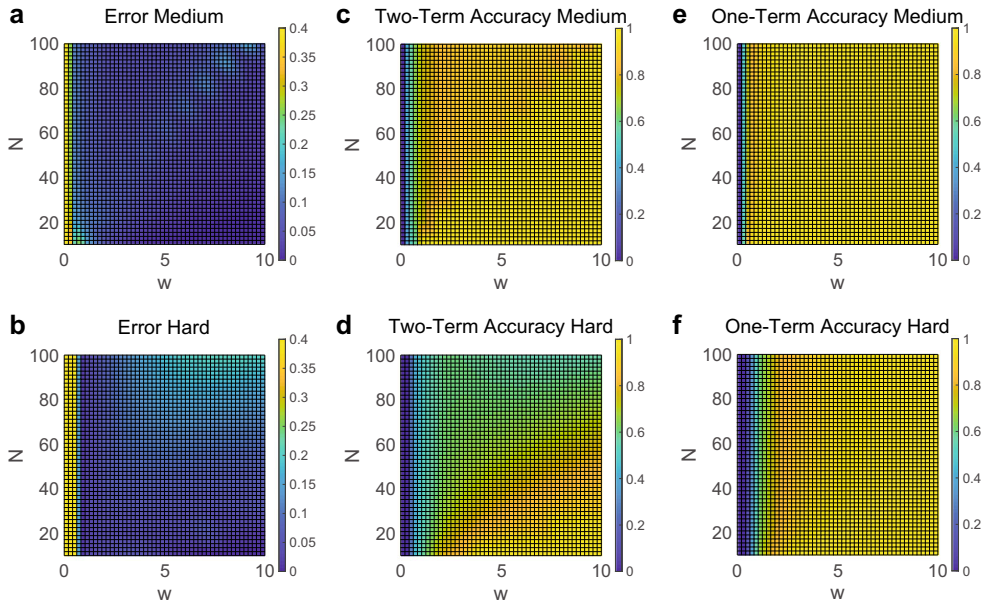

Fig. 5 **Accuracy approximation via asymptotic analysis. a–b** Relative error in the high sigmoidal steepness fixed point approximation determined using the difference in decision-making accuracy computed via the two-term asymptotic expansion for the fixed point of Eq. (5) and the numerically computed decision-making accuracy for medium and hard difficulties, respectively. **c–d** Decision-making accuracy computed via the two-term asymptotic expansion for the fixed points of Eq. (5) for medium and hard difficulties, respectively. **e–f** Decision-making accuracy computed via the one-term asymptotic expansion for the fixed points of Eq. (5) for medium and hard difficulties, respectively. Asymptotic expansions were computed for the network model with sigmoidal gain in the high steepness limit. In each panel, steepness $k=15$ was utilized for concreteness. The number of alternatives, N, and lateral inhibition strength, w, were varied in each case

To underline the impact of sigmoidal steepness, we plot in Fig. 5c and d the accuracy computed using the two-term asymptotic expansion and in Fig. 5e and f the accuracy using only the leading order term for tasks of medium and hard difficulty. We observe that the two-term expansion, incorporating the effects of finite steepness, yields lower accuracy over a broad spectrum of N and w. Thus, based on the form of the correction term in the expansion, we conclude more gradual gain functions yield decreased decision-making fidelity, though marginally so in the high-steepness limit.

Investigating the effect of k for sigmoidal gain of relatively small steepness, we depict in Fig. 6 the accuracy computed via numerical simulation for $k = 1, 2, 4$, and 10. Even outside of the high-steepness regime, we affirm that increasing gain function steepness still generally results in increased accuracy. However, for sufficiently high k, (i.e., $k > 10$) further increasing gain function steepness has negligible impact on decision-making accuracy, yielding performance analogous to binary gain. At the same time, as shown analogously in Fig. 7, a steeper gain function causes the system to require additional time in order to reach a steady-state. Thus, there exists a trade-off between decision-making accuracy and response time with gain function steepness. Nevertheless, as we will discuss in Section 3.4, the robustness of the more gradual sigmoidal gain function likely suggests that it is more favorable across decision-making tasks. It is also important to note that, as shown in Fig. 6, the optimal lateral inhibition regime for sigmoidal gain, discussed in Section 4, exists for a wide range of relatively low k, further highlighting the utility of more gradual integration of information.

3.4 Robustness to noise and attacks

The dynamics of neuronal clusters participating in the decision-making process are subject to noise and their connectivity is impacted by potential degradation over time,

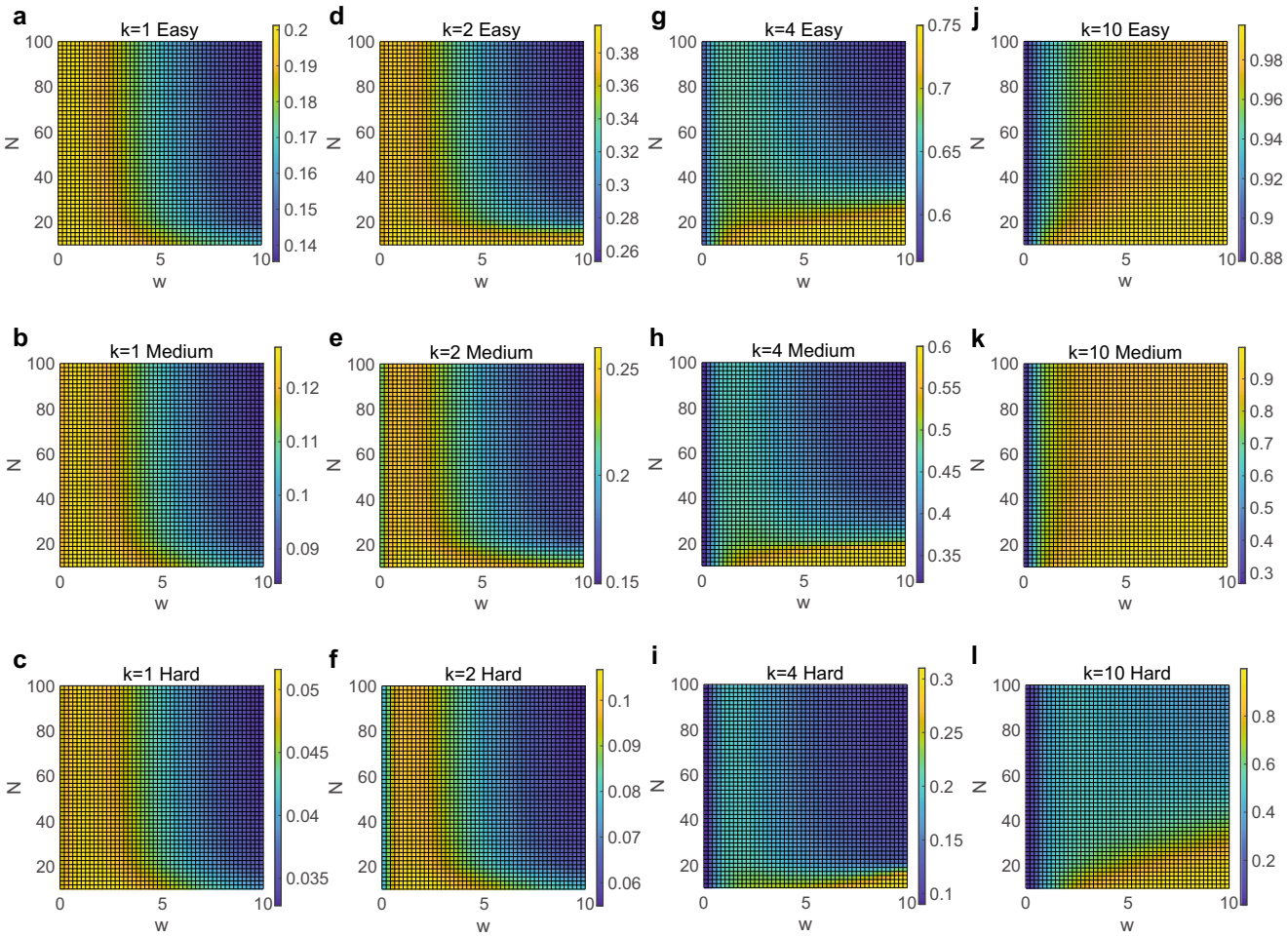

Fig. 6 Gain function steepness and accuracy. Numerically computed accuracy dependence on the number of alternatives, N, and lateral inhibition strength, w, for sigmoidal steepness: **a–c** $k = 1$, **d–f** $k = 2$, **g–i** $k = 4$, and **j–l** $k = 10$ for easy, medium, and hard difficulties, respectively. Each network is fully-connected and the accuracy averaged over 100 fair initial conditions is depicted

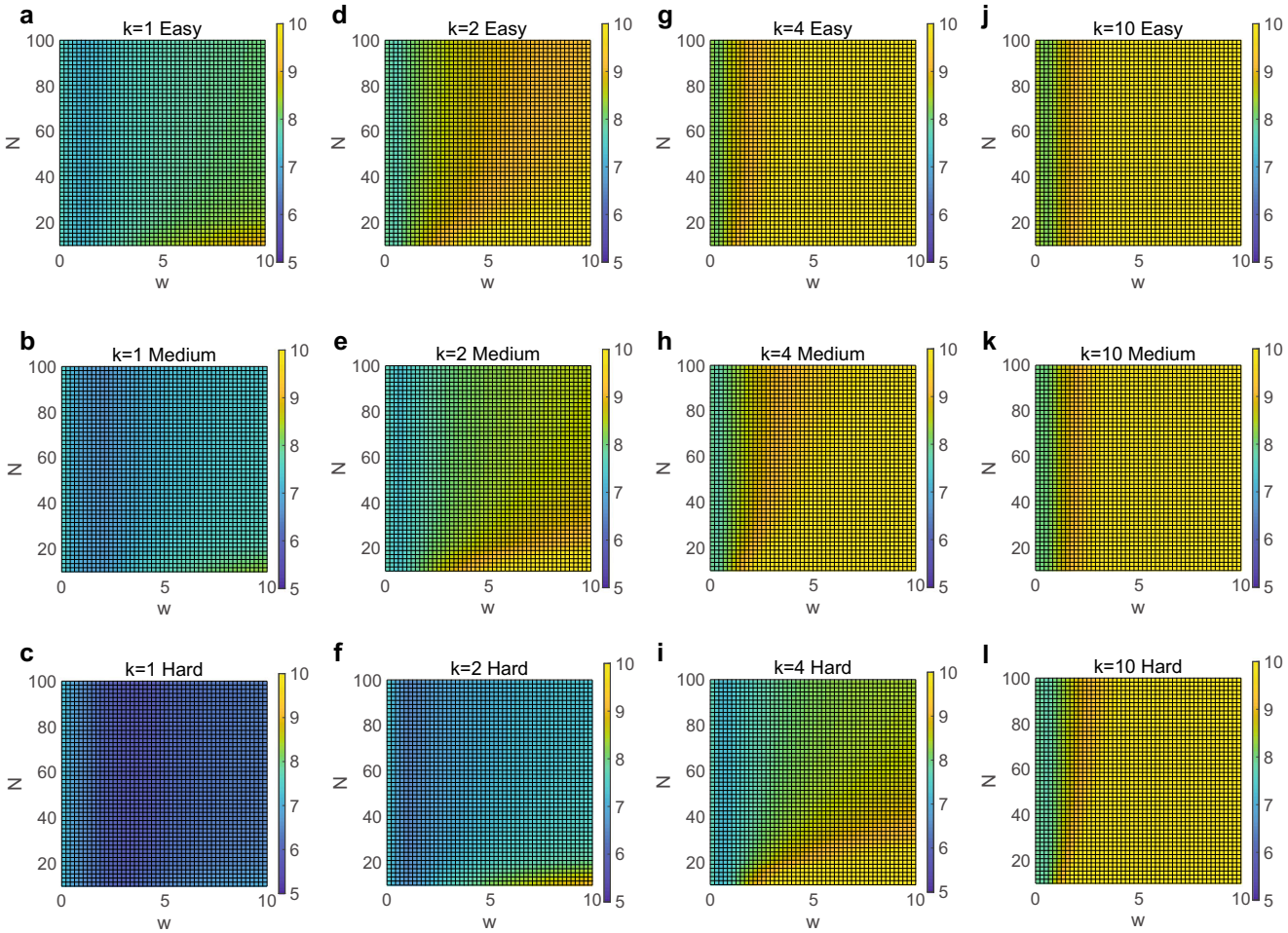

Fig. 7 Gain function steepness and response time. Numerically computed response time dependence on the number of alternatives, N, and lateral inhibition strength, w, for sigmoidal steepness: **a–c** $k = 1$, **d–f** $k = 2$, **g–i** $k = 4$, and **j–l** $k = 10$ for easy, medium, and hard difficulties, respectively. Each network is fully-connected and the response time averaged over 100 fair initial conditions is depicted

necessitating a decision-making mechanism that is largely invariant to perturbations in system conditions. Biophysical sources of noise in decision making, such as stochasticity in neuronal firing, variation in internal state, environmental effects, and transduction of sensory information (Dunn and Rieke 2006; Faisal et al. 2008; London et al. 2010), are typically averaged over or ignored in deterministic firing rate models, though we may extend our modeling framework to incorporate noisy dynamics in the context of a system of stochastic differential equations. The noisy competing firing rate network model is analogously determined by

$$dx_i = \left[-x_i + f\left(-\sum_{\substack{j=1 \\ j\neq i}}^{N} \frac{w}{p(i)} A_{ij} x_j + S_i \right) \right] dt + \sigma dW_i, \tag{13}$$

where $W_i(t)$ is a Wiener process of standard deviation σ forcing the ith neuronal assembly, thereby yielding independent, zero-mean noise injected into each cluster of neurons. Note that since the model is now stochastic, a stationary state cannot analogously be used to determine the time at which accuracy is measured as in the deterministic counterpart. Instead, the accuracy is measured after sufficient time elapses, at which point a decision is forced, as in an interrogation task.

We investigate the impact of noise on decision-making accuracy by adjusting σ, which determines the strength of the noise, across the $w - N$ parameter space. In Figs. 8 and 9, we compare the performance of the all-to-all network with sigmoidal and binary gain functions, respectively, for various choices of σ for a task of medium difficulty. Comparing the two gain function types, we observe that the network with sigmoidal gain is more robust to noise, demonstrating nearly no degradation in performance until strong noise with $\sigma > 2^{-4}$ is injected in the medium difficulty case. For the network model with binary gain, we see an immediate qualitative shift in the accuracy structure, with a broad region of parameter space shifting from nearly

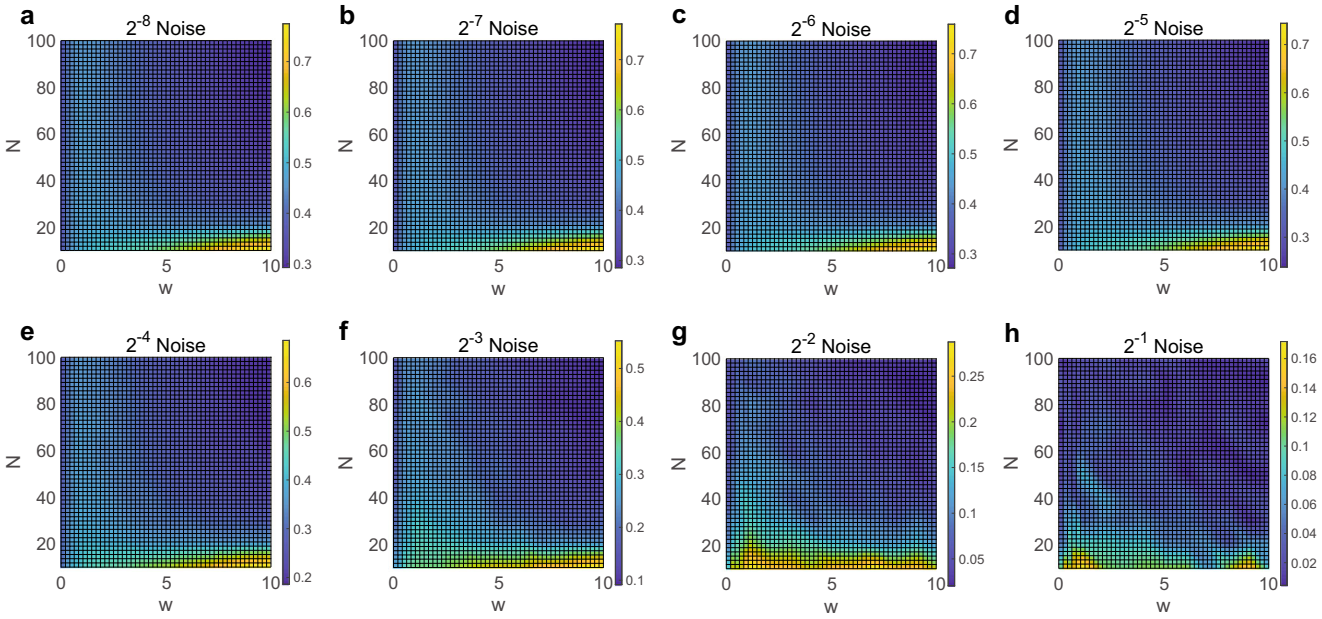

Fig. 8 Impact of noise on accuracy for networks with sigmoidal gain and medium difficulty tasks. Numerically computed accuracy dependence on number of alternatives, N, and lateral inhibition strength, w, for a fully-connected network with sigmoidal gain and noise of strength: **a** $\sigma = 2^{-8}$, **b** $\sigma = 2^{-7}$, **c** $\sigma = 2^{-6}$, **d** $\sigma = 2^{-5}$, **e** $\sigma = 2^{-4}$, **f** $\sigma = 2^{-3}$, **g** $\sigma = 2^{-2}$, and **h** $\sigma = 2^{-1}$. Each plot depicts the accuracy averaged over 100 fair initial conditions and tasks of medium difficulty

perfect to almost zero accuracy even for weak noise in which $\sigma = 2^{-8}$. The optimal span of small lateral inhibition strength for the network with sigmoidal gain also persists for weak to moderate noise strength up through approximately $\sigma = 2^{-3}$, underlining the resilience of the operating regime. For either gain function, once the noise becomes

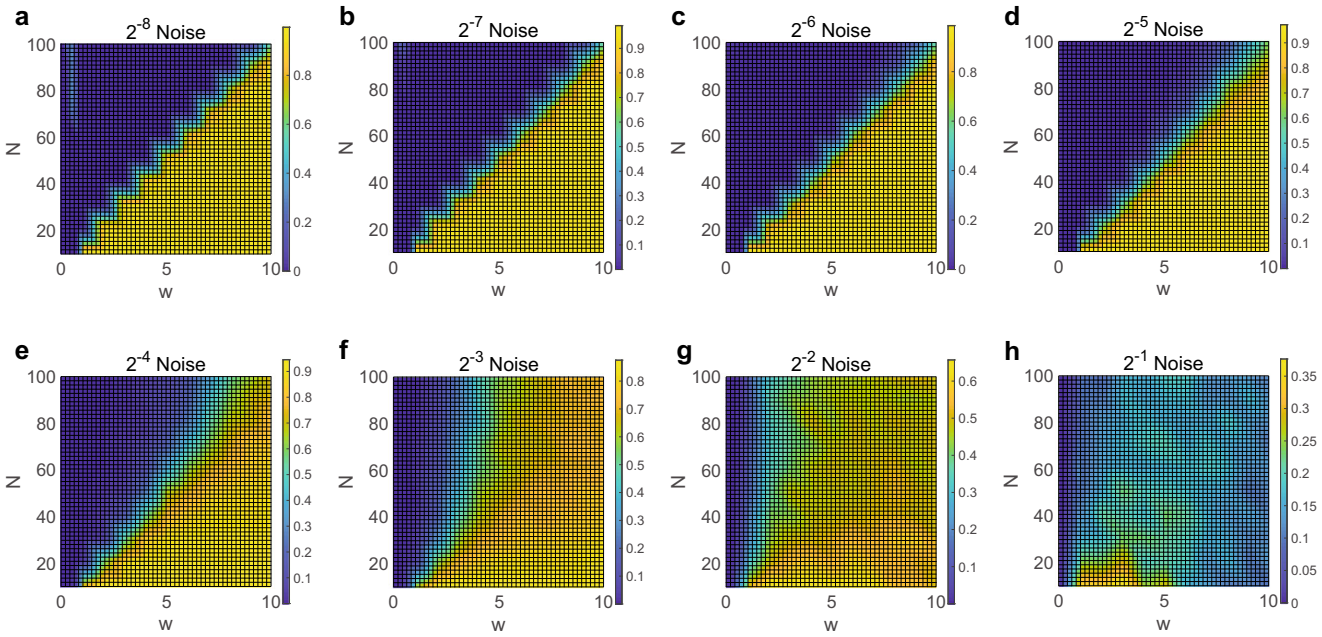

Fig. 9 Impact of noise on accuracy for networks with binary gain and medium difficulty tasks. Numerically computed accuracy dependence on number of alternatives, N, and lateral inhibition strength, w, for a fully-connected network with binary gain and noise of strength: **a** $\sigma = 2^{-8}$, **b** $\sigma = 2^{-7}$, **c** $\sigma = 2^{-6}$, **d** $\sigma = 2^{-5}$, **e** $\sigma = 2^{-4}$, **f** $\sigma = 2^{-3}$, **g** $\sigma = 2^{-2}$, and **h** $\sigma = 2^{-1}$. Each plot depicts the accuracy averaged over 100 fair initial conditions and tasks of medium difficulty

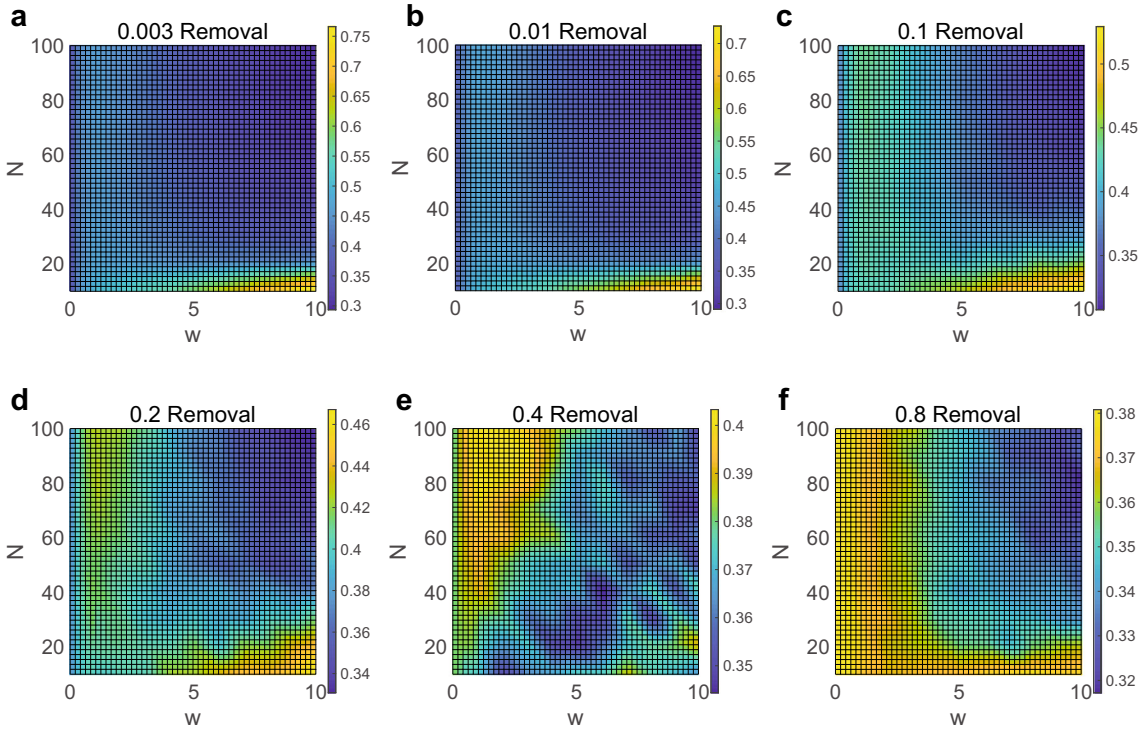

Fig. 10 Impact of connection removal on accuracy for networks with sigmoidal gain and medium difficulty tasks. Numerically computed accuracy dependence on number of alternatives, N, and lateral inhibition strength, w, for a fully-connected network with sigmoidal gain and connection removal of probability: **a** 0.003, **b** 0.01, **c** 0.1, **d** 0.2, **e** 0.4, and **f** 0.8. Each plot depicts the accuracy averaged over 100 fair initial conditions and tasks of medium difficulty

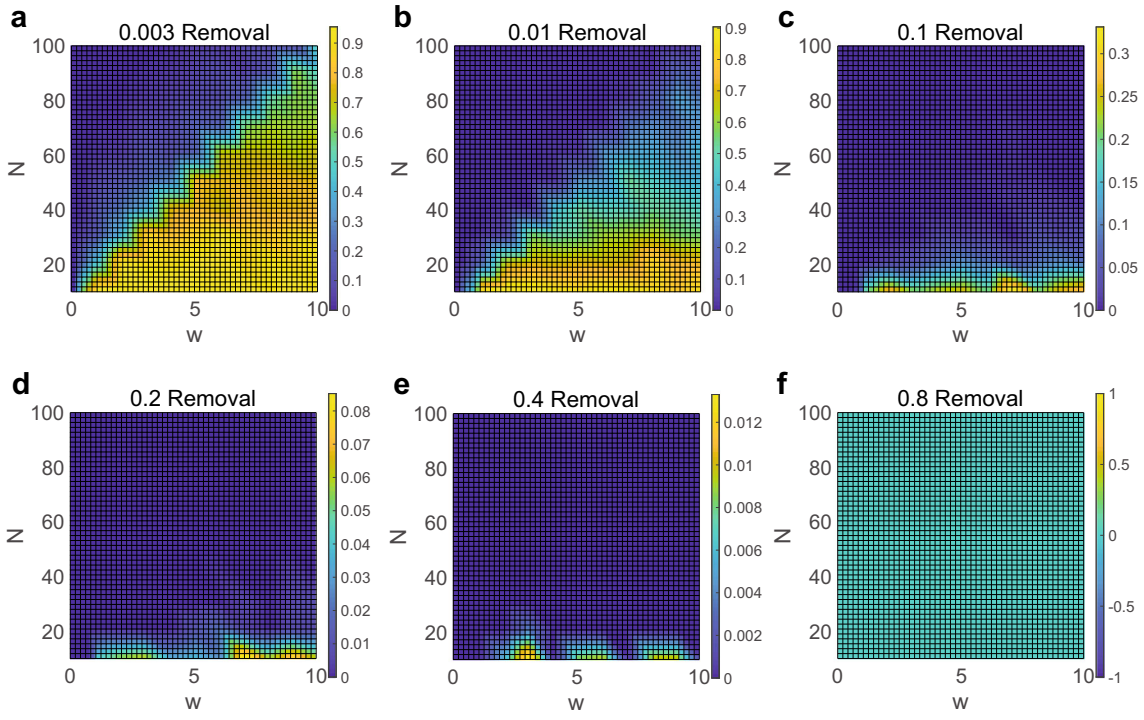

Fig. 11 Impact of connection removal on accuracy for networks with binary gain and medium difficulty tasks. Numerically computed accuracy dependence on number of alternatives, N, and lateral inhibition strength, w, for a fully-connected network with binary gain and connection removal of probability: **a** 0.003, **b** 0.01, **c** 0.1, **d** 0.2, **e** 0.4, and **f** 0.8. Each plot depicts the accuracy averaged over 100 fair initial conditions and tasks of medium difficulty

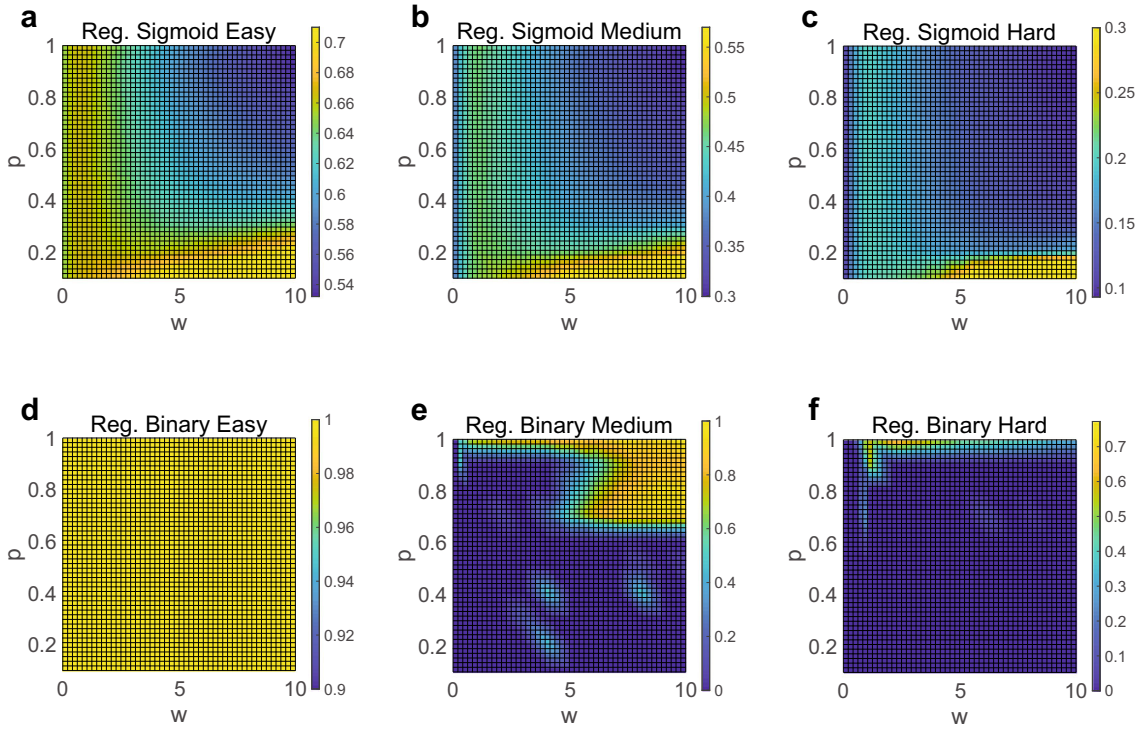

Fig. 12 Decision-making dynamics for networks with regular connectivity. a–c Numerically computed accuracy dependence on the connection density, p, and lateral inhibition strength, w, for a network with regular connectivity and sigmoidal gain for tasks of easy, medium, and hard difficulty, respectively. **d–f** Analogous plots for a network with regular connectivity and binary gain. Each plot depicts the accuracy for $N = 300$ neuronal clusters averaged over 100 fair initial conditions

sufficiently strong, overpowering the deterministic portion of the dynamics, the integrated evidence becomes less significant and the system generally exhibits low accuracy.

In a similar vein, it is important for a decision-making system to function well even if connections are removed through, for example, damage to a brain area or synaptic pruning (Manes et al. 2002; Craik and Bialystok 2006). We analyze the robustness of the model dynamics to perturbations in connectivity by randomly removing connections with increasing probability from an all-to-all network and computing the decision-making accuracy using the resultant model dynamics prescribed by Eq. (1). In Figs. 10 and 11, we plot the accuracy over the $w - N$ parameter space for a medium difficulty task when connections are removed with increasing probability using sigmoidal and binary gain functions, respectively. For the network model with sigmoidal gain, we observe a relatively slow and gradual decrease in accuracy as additional connections are removed, maintaining a qualitatively similar dependence on the number of alternatives and lateral inhibition strength in each case. As with injected noise, high accuracy is generally achieved for a stable range of small lateral inhibition strengths across connection removals. Using instead the binary gain function, we see an immediate and rapid drop in accuracy across a large range of w and N even after only a small proportion of 0.003 network connections are removed. The impact of noise and connection removal for a hard difficulty task is similar and is depicted in the Appendix C. Together, we conclude that the competing firing rate model with sigmoidal gain is robust to perturbations in both network structure and dynamics, indicating that while binary gain may yield highest accuracy for an idealized fully-connected network, its performance quickly diminishes for alternative scenarios and thus was likely not selected across the broad decision-making scenarios encountered throughout the evolution of species.

3.5 Alternative network structures

We conclude by analyzing the decision-making dynamics in our model framework for several canonical net-

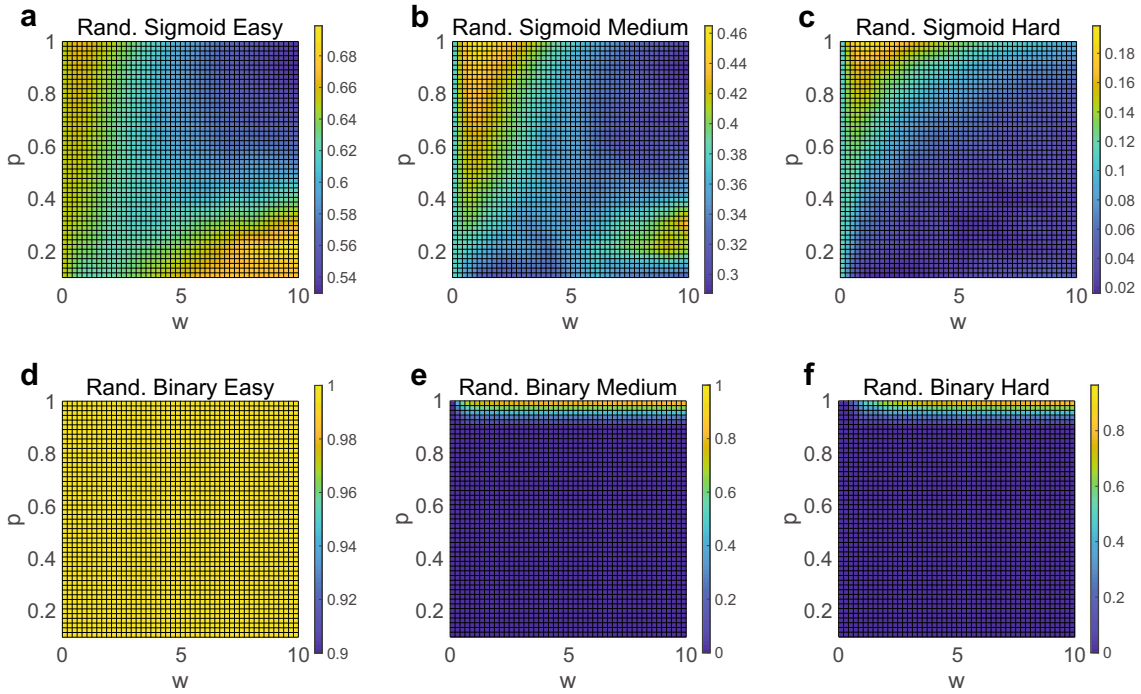

Fig. 13 Decision-making dynamics for networks with random connectivity. a–c Numerically computed accuracy dependence on the connection density, p, and lateral inhibition strength, w, for a network with random connectivity and sigmoidal gain for tasks of easy, medium, and hard difficulty, respectively. **d–f** Analogous plots for a network with random connectivity and binary gain. Each plot depicts the accuracy for $N = 300$ neuronal clusters averaged over 100 fair initial conditions

work structures beyond all-to-all connectivity. While the fully-connected network discussed in previous sections was amenable to theoretical analysis and typically used in pre-existing decision-making models, relatively sparse network connectivity with more intricate structure has been observed on both small and large scales in the brain and significantly determines the evoked network dynamics (van den Heuvel et al. 2008; Sporns and Honey 2006; Roxin et al. 2004; Barranca et al. 2015b; Markov et al. 2013). Depending on their graph structure, networks can be described through a wealth of characterizations (Markov et al. 2013; Erdos and Renyi 1959; Barranca et al. 2015a). Here we focus on networks with varying degrees of randomness and diverse connection densities, studying decision-making

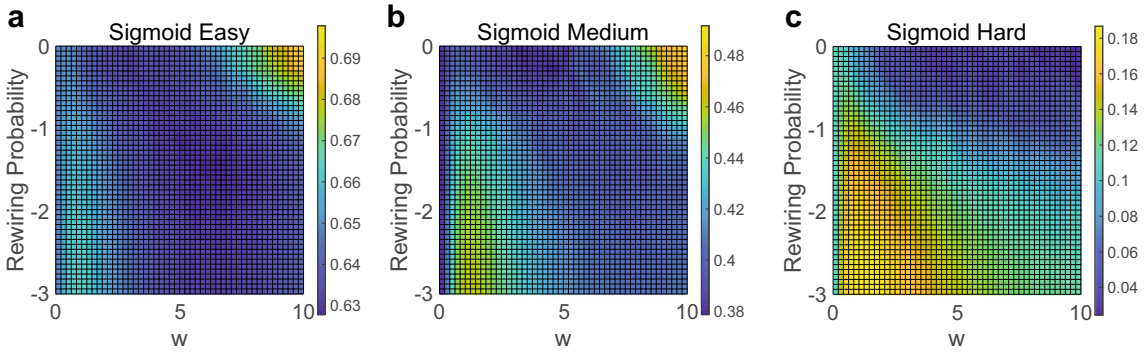

Fig. 14 Decision-making dynamics for networks across connectivity structures. a–c Numerically computed accuracy for a network with inhibition strength, w, and connectivity determined by randomly rewiring connections in a regular network with a prescribed rewiring probability for tasks of easy, medium, and hard difficulty, respectively. Each plot depicts the accuracy for $N = 300$ neuronal clusters, connection density $p = 0.1$, and sigmoidal gain averaged over 100 fair initial conditions

accuracy in the context of regular, random, and small-world connectivity.

We first investigate dynamics on a regular ring lattice of mean degree k such that neuronal clusters are connected to their nearest $k/2$ neighbors. Analogous to our previous analysis, we investigate model accuracy as the lateral inhibition strength is varied along with mean connection density, p, which prescribes the degree across the network. For concreteness, we fix the network size in this section at $N = 300$, with sufficiently many nodes to yield robust connectivity statistics in the randomly generated networks that we analyze next. In Fig. 12a–c, we depict the accuracy for networks with regular connectivity and sigmoidal gain for tasks of easy, medium, and hard difficulty, respectively. We similarly plot the accuracy for networks with regular connectivity and binary gain in Fig. 12d–f. In the case of sigmoidal gain, we see relatively high and comparable accuracy across connection densities for each task difficulty in the optimal span of low inhibition strengths. For the regular network with binary gain, reasonable accuracy is generally only achieved for high connection densities, near all-to-all connectivity, in the cases of medium and hard difficulty tasks. It is significant to remark that the accuracy achieved via sparse connectivity with sigmoidal gain is near that which is obtained with all-to-all connectivity, indicating a less connected network may be evolutionarily advantageous since it still produces high accuracy with less interactions and potentially less energy expenditure. Note that while we also observe high accuracy using sigmoidal gain for very sparse connectivity and high w, the necessary w grows with network size and is therefore not likely physiological.

Turning now to a complementary network topology, we analyze decision-making dynamics on networks with random connectivity. In this case, each pair of nodes is randomly and independently connected with probability p. In Fig. 13a–c, we vary the lateral inhibition strength and connection density for such random networks, plotting the resultant accuracy using sigmoidal gain across tasks of easy, medium, and hard difficulties. The related plots using binary gain are depicted in 13d–f. Though the connectivity structure is entirely distinct from the regular connectivity case, the results are still qualitatively similar. The random network with sigmoidal gain demonstrates high accuracy for low w over a range of connection densities 0.1 or higher. As in the regular case, the random network with binary gain only displays accurate decision making for high connection densities near $p = 1$ in non-simple tasks, indicating a lack of robustness for networks with more physiological connectivity.

Comparing the overall performance for the regular and random network topologies, we observe that the regular network with sigmoidal gain generally exhibits higher accuracy across connection densities. We have verified empirically that the network clustering coefficient, as opposed to, for example, average shortest path length, is a good predictor of decision-making accuracy, well aligning with the higher accuracy of the regular network. To more thoroughly examine the role of randomness and regularity in decision-making networks, we analyze the accuracy for connectivity structures that interpolate between the two extremes. In particular, we randomly rewire connections in the regular lattice with rewiring probability β, removing links from the lattice and randomly placing a new connection between two originally nonadjacent nodes in each rewire. Thus, networks with larger rewiring probability display more randomness in their connectivity structure. For intermediate rewiring probabilities, in the approximate range of $0.01 \leq \beta \leq 0.1$, such networks are considered small-world and demonstrate simultaneously high clustering and short path lengths, thereby exhibiting advantageous properties of regular and random networks, respectively (Watts and Strogatz 1998).

In Fig. 14a–c, we plot the decision-making accuracy dependence on the rewiring probability and lateral inhibition strength for networks with sigmoidal integration of evidence and fixed low connection density as common in small-world networks. We observe across levels of randomness and task difficulty that relatively high accuracy is achieved for the same range of low lateral inhibition strengths as identified in previous sections. Note that in the case of binary gain, 0 accuracy is yielded across such network configurations for tasks of medium and hard difficulty, largely due to multiple winning nodes, and thus these results are omitted from Fig. 14. Examining the optimal connectivity structure for decision-making performance across choices of w using sigmoidal gain, networks with regular or small-world connectivity exhibit the highest accuracy overall. This is consistent with the analysis of purely regular and random networks across connection densities, underlining clustering of neuronal assemblies as a key facet in decision making. Though networks with high connection density generally demonstrate high clustering automatically and corresponding robust performance in decision making, such dense connectivity is likely inconsistent with the limitations on energy consumption, rapid information processing, and functional separation selected by evolution (Bogacz et al. 2007; Douglas and Martin 2007; Sporns and Honey 2006). We hypothesize that more sparsely connected clusters of neuronal assemblies, in the form of small-world

networks, for example (van den Heuvel et al. 2008; Sporns and Honey 2006; Roxin et al. 2004), optimally balance accuracy and efficiency in decision-making tasks.

4 Discussion

Through analysis of our competing firing rate network model, we provide a novel characterization of the interplay between information integration structure, network connectivity, and the accuracy as well as robustness of decision making for tasks that potentially involve a large number of alternatives. We underline the existence of a dynamical regime signified by weak lateral inhibition that broadly achieves optimal accuracy across task difficulties, numbers of task alternatives, reasonably noisy conditions, and network structures. Such desirable decision-making dynamics are energetically efficient and agree with fundamental physiological observations. For networks that demonstrate excessively steep integration of evidence, however, we observe a lack of robustness in terms of the stability of an optimal parameter regime in addition to poor resistance to noise and changes in network structure. For sufficiently large lateral inhibition strength, which grows with the number of task alternatives, we do observe high decision-making accuracy for systems with nearly binary gain at the price of increased response time, demonstrating a speed-accuracy trade-off as commonly observed in psychological studies (Fitts 1966; Bogacz et al. 2010). Diverging levels of activity in neuronal clusters via attractor dynamics is well documented for decision making in experimental settings, particularly for visual search, virtual navigation, and reaching tasks (Thomas and Pare 2007; Cohen et al. 2010; Harvey et al. 2012; Churchland et al. 2012), and thus our analysis serves to gain deeper insight into the mechanisms and evolutionary benefits of such neuronal computations in the context of a biologically plausible yet idealized model network setting.

Our network analysis demonstrates that systems with a mixture of randomness and regularity in their structure, as typically observed in experiment, are able to robustly perform decision-making tasks utilizing sigmoidal integration of evidence. However, for systems with excessively random structure, degradation in accuracy is incurred, particularly for more difficult tasks. These results suggest that evolution has selected decision-making systems with relatively sparse and modular structure among neuronal assemblies with relatively gradual integration of information, thereby achieving parsimonious and profitable outcomes across a large ensemble of conditions.

Impaired decision making is believed to play a fundamental role in a variety of mental disorders, including obsessive-compulsive behavior, autism, and several forms of anxiety (Sachdev and Malhi 2005; Fellows 2004), and thus understanding the neural mechanisms of choice has important implications in human health. Our work suggests that particularly rapid integration of information or perturbations in the circuitry connecting neuronal assemblies could potentially contribute to such decision-making disorders. Recent experimental studies suggest the existence of a neural system that identifies task difficulty and modulates resources necessary in order to accurately choose among alternatives (Heekeren et al. 2008), and, in the context of our theoretical observations, we hypothesize that increased functional connectivity among neuronal clusters, akin to a more highly connected network, is consistent with improved decision making via larger utilization of energetic resources.

While we studied the decision-making dynamics for a neural system using two plausible classes of gain functions and several representative network structures, experimental data may also be used in conjunction with our model framework to guide future investigations upon, for example, obtaining more physiological approximations of neuronal cluster response functions or recovering the connectivity between neuronal assemblies (Kumar and Penny 2014; La Camera et al. 2006; Markov et al. 2013). Reconciling our macroscale competing firing rate network model with the dynamics of biologically realistic neurons at the individual level also marks an interesting area of future analysis. There is experimental evidence for alternative classes of attractors in cortical decision-making systems, ranging from line attractors in area LIP (Gold and Shadlen 2002; Brody et al. 2003; Ganguli et al. 2008) to ring attractors in head-direction systems (Taube 2007; Xie et al. 2002); while our work primarily focused on decision-making dynamics via point attractors, exhibiting a unique asymptotically stable fixed point for a given choice of model parameters, alternative nonlinear dynamical system models may be analogously investigated for cortical areas demonstrating low-dimensional attractors. With a continuum of potential attracting fixed points, and corresponding decisions depending on the initial state of the system, network models with more complicated attractor structures may give insights into the encoding of continuous decision-making information as well as working memory.

Grounded in analog rate-based encoding of evidence at steady-state, our network model demonstrates accurate winner-take-all behavior across biologically plausible settings. While taking the minimal state space for individual neurons to be binary, determined by the presence or absence of firing events, is consistent with our neuronal-assembly-based decision-making framework in prescribing a firing rate function for each cluster, our work indicates that such binary state thresholding at the level of neuronal assemblies is potentially counterproductive to robust decision making. Though modern technology largely utilizes binary encoding

of information, biological constraints and a vast repertoire of task conditions have likely pushed evolution towards more continuous decision-making mechanisms, highlighting the importance of engineering novel systems which operate under principles that reflect neuronal network computation.

Acknowledgements This work was supported by NSF grant DMS-1812478 and a Swarthmore Faculty Research Support Grant.

Compliance with Ethical Standards

Conflict of interests The authors declare that they have no conflict of interest.

Appendix A: Uniqueness of Fixed Point with Sigmoidal Gain

In this section of the Appendix, we provide a justification for the sufficient conditions guaranteeing a unique fixed point in the all-to-all network with sigmoidal gain discussed in Section 3.1.1, which we restate below.

Uniqueness of Fixed Point with Sigmoidal Gain: The decision-making network model given in Eq. (1) with sigmoidal gain function f as prescribed by Eq. (2) has a unique fixed point if there exists positive constant M such that $f'(x_i) \leq M, \forall x_i$, and $\frac{wM}{N-1} < 1$ for $i = 1, \ldots, N$.

We consider fixed points $x^* = (x_1^*, x_2^*, \ldots, x_N^*)$ and $x' = (x_1', x_2', \ldots, x_N')$ for Eq. (1), and demonstrate that $x^* = x'$ if $\frac{wM}{N-1} < 1$. Let $u_i = x_i' - x_i^*$ denote the difference between the ith components of the fixed points. Since x' is a fixed point, it follows that $x_i' = f(-\sum_{j\neq i} \frac{w}{N-1} x_j' + S_i)$. Hence,

$$x_i^* + u_i = f\left(-\sum_{j\neq i} \frac{w}{N-1} x_j^* + S_i - \sum_{j\neq i} \frac{w}{N-1} u_j\right). \tag{14}$$

Since f is smooth, according to the mean value theorem

$$f\left(-\sum_{j\neq i} \frac{w}{N-1} x_j^* + S_i - \sum_{j\neq i} \frac{w}{N-1} u_j\right)$$
$$= f\left(-\sum_{j\neq i} \frac{w}{N-1} x_j^* + S_i\right) + f'(c_i)\left(-\sum_{j\neq i} \frac{w}{N-1} u_j\right),$$

where c_i is contained in open interval $(-\sum_{j\neq i} \frac{w}{N-1} x_j^* + S_i - \sum_{j\neq i} \frac{w}{N-1} u_j, -\sum_{j\neq i} \frac{w}{N-1} x_j^* + S_i)$. Given x_i^* is a fixed point, we re-express Eq. (14) as

$$x_i^* + u_i = f\left(-\sum_{j\neq i} \frac{w x_j^*}{N-1} + S_i\right) + f'(c_i)\left(-\sum_{j\neq i} \frac{w u_j}{N-1}\right)$$
$$\implies u_i = -\frac{w}{N-1} f'(c_i)\left(\sum_{j\neq i} u_j\right).$$

Labeling $a_i = \frac{w}{N-1} f'(c_i)$ for notational convenience, it follows $u_i + a_i \sum_{j\neq i} u_j = 0$. We can rewrite this compactly in matrix notation as $Au = 0$, where

$$A = \begin{bmatrix} 1 & a_1 & a_1 & \ldots & a_1 \\ a_2 & 1 & a_2 & \ldots & a_2 \\ a_3 & a_3 & 1 & \ldots & a_3 \\ \vdots & \vdots & \vdots & \ddots & \vdots \\ a_N & a_N & a_N & \ldots & 1 \end{bmatrix},$$

and $\det(A) = \prod_{k=1}^{N}(1-a_k) + \sum_{i=1}^{N} a_i \prod_{k\neq i}(1-a_k)$ (Horn and Johnson 2012).

Finally, assuming $f'(x_i) \leq M, \forall x_i$, and $\frac{w}{N-1} M < 1$, it follows that $a_i = \frac{w}{N-1} f'(c_i) \leq \frac{w}{N-1} M < 1$. As a result, $\det(A) \neq 0$, and the linear system $Au = 0$ has a unique solution $u = 0$. This implies that $x' = x^*$, demonstrating the fixed point is indeed unique.

Appendix B: Global Attraction to the Perturbed Fixed Point with Binary Gain

In Appendix B, we provide a justification for the conditions guaranteeing the existence and global attraction of the perturbed fixed point in the all-to-all network with binary gain discussed in Section 3.1.2, which we restate below.

Global Attraction to the Perturbed Fixed Point with Binary Gain: For non-simple and fair tasks with number of alternatives $N \geq 3$, the reduced decision-making network model given in Eq. (5) with binary gain function f as prescribed by Eq. (3) is globally attracted to the perturbed fixed point such that

$$\lim_{t\to\infty} x_w = 1, \tag{6a}$$

$$\lim_{t\to\infty} x_l \in [z, z+\epsilon), \tag{6b}$$

for any $\epsilon > 0$ under assumptions

$$N > \max\left(\frac{2w - (S_l - b)}{w - (S_l - b)}, \frac{w}{S_l - b} + 1\right), \tag{7a}$$

$$w > S_l - b, \tag{7b}$$

where

$$z = \frac{(N-1)(S_l - b) - w}{(N-2)w}. \tag{8}$$

Under assumptions (7), we first show that it is impossible for $\frac{dx_l}{dt} = 0$ and thus impossible for stationary dynamics to be reached. If $\frac{dx_l}{dt} = 0$, then either (i) $x_l = 0$ and $f\left(-wx_l - \frac{w}{N-1}(x_w - x_l) + S_l\right) = 0$, or (ii) $x_l = 1$ and $f\left(-wx_l - \frac{w}{N-1}(x_w - x_l) + S_l\right) = 1$. We verify that neither of these cases are possible. Case (i) requires $x_w > \frac{(S_l-b)(N-1)}{w}$, but assumption (7a) requires $w < (S_l - b)(N-1)$, forcing $x_w > 1$ and making this potential fixed point impossible. Case (ii) requires $-wx_l - \frac{w}{N-1}(x_w - x_l) + S_l \geq b$, making $x_w \leq \frac{(S_l-b)(N-1)}{w} + 1 - (N-1)$. However, assumption (7b) requires that $(N-1) > \frac{(S_l-b)(N-1)}{w} + 1$, forcing $x_w < 0$, which is impossible.

Next, to determine the state around which the system gravitates after a long time horizon, we show $z_l = \frac{(N-1)(S_l-b)-wx_w}{(N-2)w}$ separates the dynamics of x_l into distinct strictly increasing and strictly decreasing regimes, such that if $x_l \leq z_l$ then $\frac{dx_l}{dt} > 0$ and if $x_l > z_l$ then $\frac{dx_l}{dt} < 0$. To see this, note that if $\frac{dx_l}{dt} > 0$, then $f\left(-wx_l - \frac{w}{N-1}(x_w - x_l) + S_l\right) = 1$ necessarily, and thus $-wx_l - \frac{w}{N-1}(x_w - x_l) + S_l \geq b$. This forces $x_l \leq \frac{(N-1)(S_l-b)-wx_w}{(N-2)w}$, which demonstrates $x_l > z_l \implies \frac{dx_l}{dt} < 0$. An analogous argument assuming instead $\frac{dx_l}{dt} < 0$ yields $x_l \leq z_l \implies \frac{dx_l}{dt} > 0$.

As a result, it is guaranteed after sufficient time elapses $x_l \to [z_l, z_l + \epsilon)$, for any $\epsilon > 0$. Since $z_l \in (0, 1)$ under assumptions (7) and $x_w \in [0, 1]$, we obtain, independent of x_w, the upper bound $z_l \leq \frac{(N-1)(S_l-b)}{(N-2)w} < \frac{S_l-b}{w}$. Thus, as $t \to \infty$, the total input into the gain function for the wth node is $-wx_l + S_w > b + (S_w - S_l) > b$, and consequently $x_w \to 1$. As a result, $x_l \to [z, z+\epsilon)$ for $z = \frac{(N-1)(S_l-b)-w}{(N-2)w}$, which gives an attracting perturbed fixed point depending only on the model parameters.

Appendix C: Robustness of Decision-Making for Hard Difficulty Tasks

In this Appendix, we provide additional figures depicting the network model decision-making dynamics subject to noise and then connection removal for hard difficulty tasks. In Figs. 15 and 16, we plot, for various choices of noise strength, the accuracy over the $w - N$ parameter space for all-to-all networks with sigmoidal and binary gain functions, respectively. Similarly, in Figs. 17 and 18, we

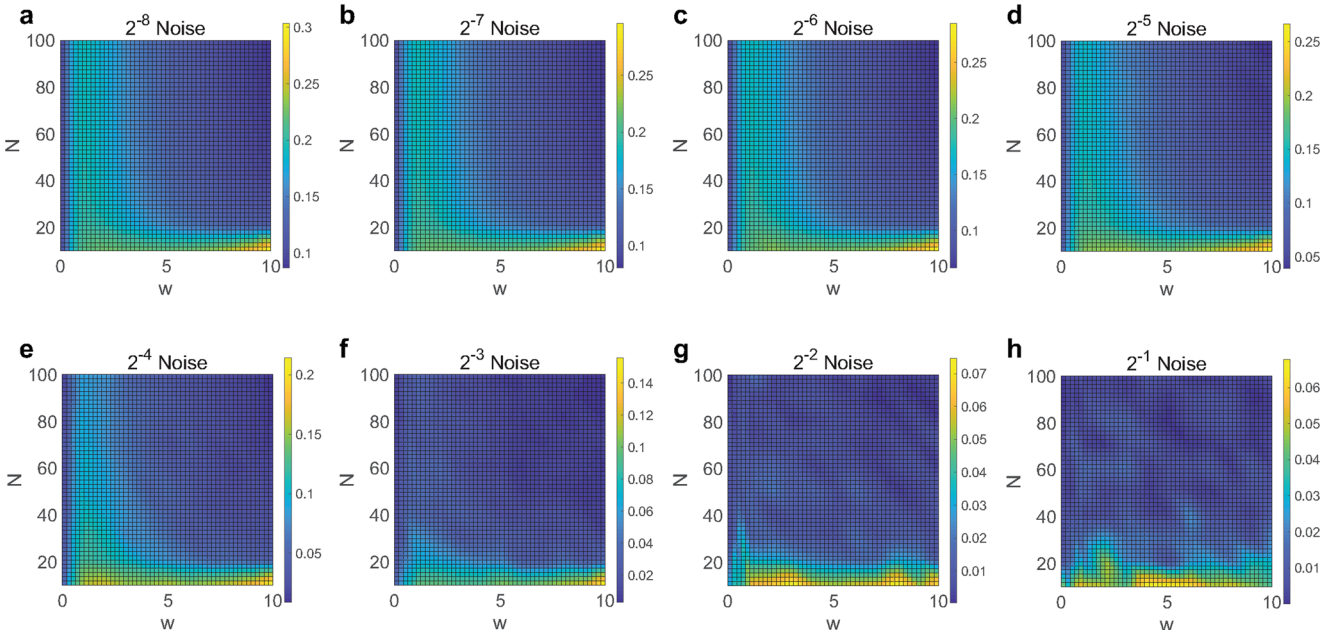

Fig. 15 Impact of noise on accuracy for networks with sigmoidal gain and hard difficulty tasks. Numerically computed accuracy dependence on number of alternatives, N, and lateral inhibition strength, w, for a fully-connected network with sigmoidal gain and noise of strength: **a** $\sigma = 2^{-8}$, **b** $\sigma = 2^{-7}$, **c** $\sigma = 2^{-6}$, **d** $\sigma = 2^{-5}$, **e** $\sigma = 2^{-4}$, **f** $\sigma = 2^{-3}$, **g** $\sigma = 2^{-2}$, and **h** $\sigma = 2^{-1}$. Each plot depicts the accuracy averaged over 100 fair initial conditions and tasks of hard difficulty

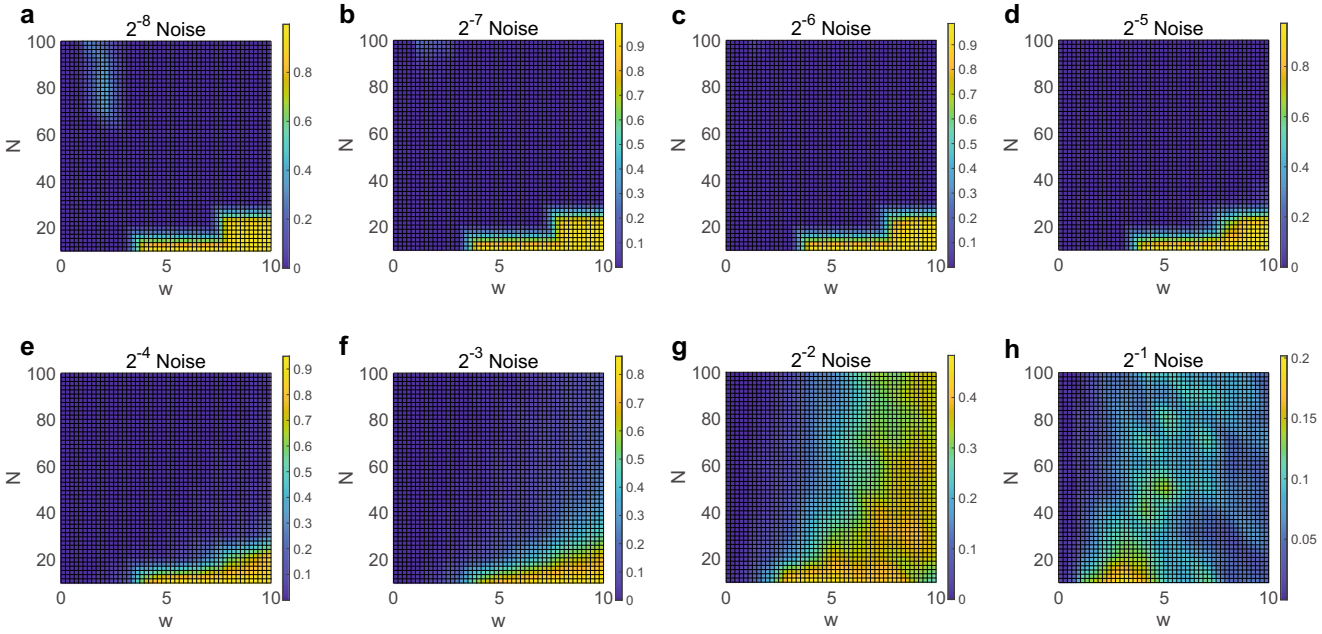

Fig. 16 Impact of noise on accuracy for networks with binary gain and hard difficulty tasks. Numerically computed accuracy dependence on number of alternatives, N, and lateral inhibition strength, w, for a fully-connected network with binary gain and noise of strength: **a** $\sigma = 2^{-8}$, **b** $\sigma = 2^{-7}$, **c** $\sigma = 2^{-6}$, **d** $\sigma = 2^{-5}$, **e** $\sigma = 2^{-4}$, **f** $\sigma = 2^{-3}$, **g** $\sigma = 2^{-2}$, and **h** $\sigma = 2^{-1}$. Each plot depicts the accuracy averaged over 100 fair initial conditions and tasks of hard difficulty

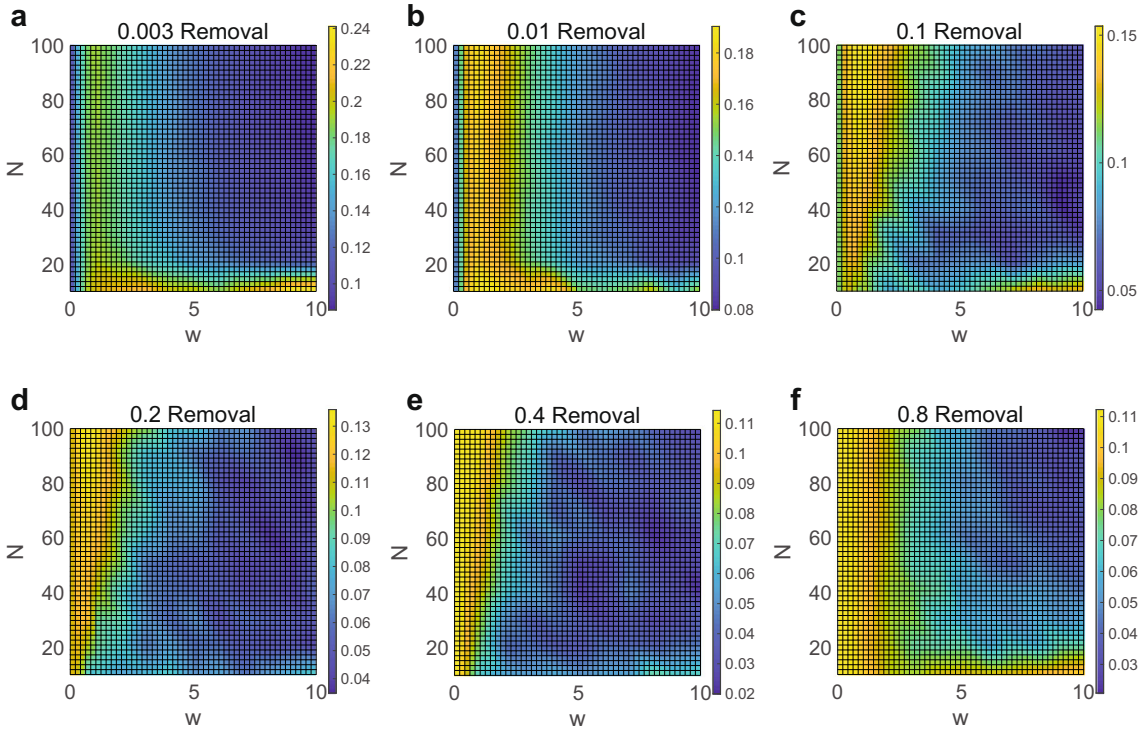

Fig. 17 Impact of connection removal on accuracy for networks with sigmoidal gain and hard difficulty tasks. Numerically computed accuracy dependence on number of alternatives, N, and lateral inhibition strength, w, for a fully-connected network with sigmoidal gain and connection removal of probability: **a** 0.003, **b** 0.01, **c** 0.1, **d** 0.2, **e** 0.4, and **f** 0.8. Each plot depicts the accuracy averaged over 100 fair initial conditions and tasks of hard difficulty

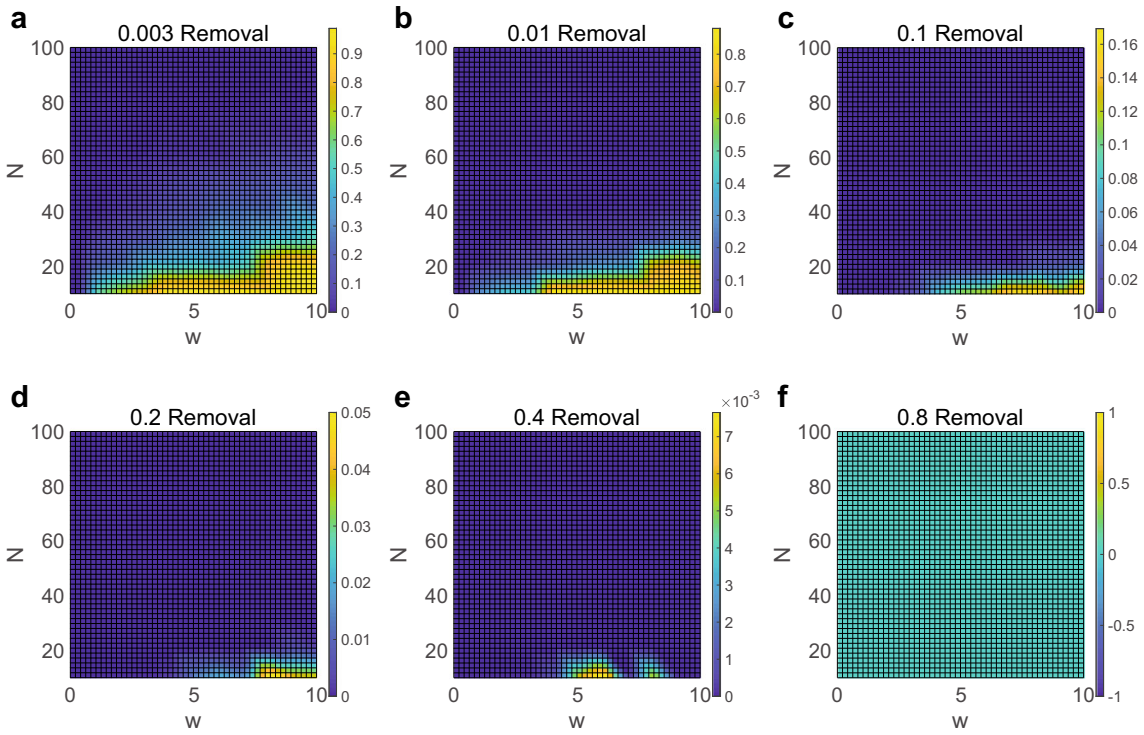

Fig. 18 Impact of connection removal on accuracy for networks with binary gain and hard difficulty tasks. Numerically computed accuracy dependence on number of alternatives, N, and lateral inhibition strength, w, for a fully-connected network with binary gain and connection removal of probability: **a** 0.003, **b** 0.01, **c** 0.1, **d** 0.2, **e** 0.4, and **f** 0.8. Each plot depicts the accuracy averaged over 100 fair initial conditions and tasks of hard difficulty

compare the decision-making performance upon randomly removing connections with increasing probability. The resultant dynamics are analogous to those evoked in the medium difficulty case discussed in detail in Section 3.4.

References

Ahmed, B., Anderson, J.C., Douglas, R.J., Martin, K.A., Whitteridge, D. (1998). Estimates of the net excitatory currents evoked by visual stimulation of identified neurons in cat visual cortex. *Cereb Cortex*, *8*(5), 462–476.

Andronov, A.A. (1973). Qualitative theory of second-order dynamic systems. A Halsted Press book. Wiley. ISBN 9780706512922.

Barranca, V.J., Zhou, D., Cai, D. (2015a). A novel characterization of amalgamated networks in natural systems. *Scientific Reports*, *5*, 10611.

Barranca, V.J., Zhou, D., Cai, D. (2015b). Low-rank network decomposition reveals structural characteristics of small-world networks. *Phys rev e stat nonlin soft matter phys*, *92*(6), 062822.

Barttfeld, P., Uhrig, L., Sitt, J.D., Sigman, M., Jarraya, B., Dehaene, S. (2015). Signature of consciousness in the dynamics of resting-state brain activity. *Proceedings of the National Academy of Sciences of the USA*, *112*(3), 887–892. ISSN 0027-8424. https://doi.org/10.1073/pnas.1418031112.

Bendixson, I. (1901). Sur les courbes definies par des equations differentielles. *Acta Math*, *24*, 1–88. https://doi.org/10.1007/BF02403068.

Binas, J., Rutishauser, U., Indiveri, G., Pfeiffer, M. (2014). Learning and stabilization of winner-take-all dynamics through interacting excitatory and inhibitory plasticity. *Frontiers in Computational Neuroscience*, *8*, 68.

Bogacz, R., Usher, M., Zhang, J., McClelland, J.L. (2007). Extending a biologically inspired model of choice: multi-alternatives, nonlinearity and value-based multidimensional choice. *Philosophical Transactions of the Royal Society of London. Series B, Biological Sciences*, *362*(1485), 1655–1670.

Bogacz, R., Wagenmakers, E.J., Forstmann, B.U., Nieuwenhuis, S. (2010). The neural basis of the speed-accuracy tradeoff. *Trends in Neurosciences*, *33*(1), 10–16.

Brody, C.D., Romo, R., Kepecs, A. (2003). Basic mechanisms for graded persistent activity: discrete attractors, continuous attractors, and dynamic representations. *Current Opinion in Neurobiology*, *13*(2), 204–211.

Brouwer, L.E.J. (1912). Über abbildung von mannigfaltigkeiten. *Mathematische Annalen*, *71*(4), 598–598. ISSN 1432-1807. https://doi.org/10.1007/BF01456812.

Churchland, M.M., Cunningham, J.P., Kaufman, M.T., Foster, J.D., Nuyujukian, P., Ryu, S.I., Shenoy, K.V. (2012). Neural population dynamics during reaching. *Nature*, *487*(7405), 51–56.

Cohen, J.Y., Crowder, E.A., Heitz, R.P., Subraveti, C.R., Thompson, K.G., Woodman, G.F., Schall, J.D. (2010). Cooperation and competition among frontal eye field neurons during visual target selection. *The Journal of Neuroscience*, *30*(9), 3227–3238.

Craik, F.I., & Bialystok, E. (2006). Cognition through the lifespan: mechanisms of change. *Trends in Cognitive Sciences (Regul. Ed.)*, *10*(3), 131–138.

Dayan, P., & Abbott, L.F. (2001). *Theoretical neuroscience*. Cambridge: MIT press.

de Lafuente, V., & Romo, R. (2006). Neural correlate of subjective sensory experience gradually builds up across cortical areas. *Proceedings of the National Academy of Sciences of the USA*, *103*(39), 14266–14271.

Deco, G., Jirsa, V.K., McIntosh, A.R. (2011). Emerging concepts for the dynamical organization of resting-state activity in the brain. *Nature Reviews. Neuroscience*, *12*(1), 43–56.

Ding, L., & Gold, J.I. (2013). The basal Ganglia's contributions to perceptual decision making. *Neuron*, *79*(4), 640–649.

Douglas, R.J., & Martin, K.A. (2007). Recurrent neuronal circuits in the neocortex. *Current Biology*, *17*(13), 496–500.

Dunn, F.A., & Rieke, F. (2006). The impact of photoreceptor noise on retinal gain controls. *Current Opinion in Neurobiology*, *16*(4), 363–370.

Erdos, P., & Renyi, A. (1959). On random graphs i. *Publicationes Mathematicae Debrecen*, *6*, 290.

Ermentrout, B. (1992). Complex dynamics in winner-take-all neural nets with slow inhibition. *Neural Networks*, *5*(3), 415–431. ISSN 0893-6080. https://doi.org/10.1016/0893-6080(92)90004-3.

Faisal, A.A., Selen, L.P., Wolpert, D.M. (2008). Noise in the nervous system. *Nature Reviews. Neuroscience*, *9*(4), 292–303.

Fellows, L.K. (2004). The cognitive neuroscience of human decision making: a review and conceptual framework. *Behavioral and Cognitive Neuroscience Reviews*, *3*(3), 159–172.

Fitts, P.M. (1966). Cognitive aspects of information processing. 3. Set for speed versus accuracy. *Journal of Experimental Psychology*, *71*(6), 849–857.

Fukai, T., & Tanaka, S. (1997). A simple neural network exhibiting selective activation of neuronal ensembles: from winner-take-all to winners-share-all. *Neural Computation*, *9*(1), 77–97.

Ganguli, S., Bisley, J.W., Roitman, J.D., Shadlen, M.N., Goldberg, M.E., Miller, K.D. (2008). One-dimensional dynamics of attention and decision making in lIP. *Neuron*, *58*(1), 15–25.

Gold, J.I., & Shadlen, M.N. (2002). Banburismus and the brain: decoding the relationship between sensory stimuli, decisions, and reward. *Neuron*, *36*(2), 299–308.

Harvey, C.D., Coen, P., Tank, D.W. (2012). Choice-specific sequences in parietal cortex during a virtual-navigation decision task. *Nature*, *484*(7392), 62–68.

He, Y., Chen, Z.J., Evans, A.C. (2007). Small-world anatomical networks in the human brain revealed by cortical thickness from MRI. *Cereb Cortex*, *17*(10), 2407–2419.

Heekeren, H.R., Marrett, S., Ungerleider, L.G. (2008). The neural systems that mediate human perceptual decision making. *Nature Reviews. Neuroscience*, *9*(6), 467–479.

Hick, W.E. (1952). On the rate of gain of information. *Quarterly Journal of Experimental Psychology*, *4*(1), 11–26. https://doi.org/10.1080/17470215208416600.

Hodgkin, A.L., & Huxley, A.F. (1952). A quantitative description of membrane current and its application to conduction and excitation in nerve. *The Journal of Physiology (Lond.)*, *117*(4), 500–544.

Hopfield, J.J. (1982). Neural networks and physical systems with emergent collective computational abilities. *Proceedings of the National Academy of Sciences of the USA*, *79*(8), 2554–2558.

Horn, R.A., & Johnson, C.R. (2012). Matrix Analysis. Cambridge University Press, 2nd edn. https://doi.org/10.1017/9781139020411.

Krizhevsky, A., Sutskever, I., Hinton, G.E. (2017). Imagenet classification with deep convolutional neural networks. *Commun. ACM*, *60*(6), 84–90. ISSN 0001-0782. https://doi.org/10.1145/3065386.

Kumar, S., & Penny, W. (2014). Estimating neural response functions from fMRI. *Frontiers in Neuroinformatics*, *8*, 48.

La Camera, G., Rauch, A., Thurbon, D., Luscher, H.R., Senn, W., Fusi, S. (2006). Multiple time scales of temporal response in pyramidal and fast spiking cortical neurons. *Journal of Neurophysiology*, *96*(6), 3448–3464.

London, M., Roth, A., Beeren, L., Hausser, M., Latham, P.E. (2010). Sensitivity to perturbations *in vivo* implies high noise and suggests rate coding in cortex. *Nature*, *466*(7302), 123–127.

Luo, T., Liu, S., Li, L., Wang, Y., Zhang, S., Chen, T., Xu, Z., Temam, O., Chen, Y. (2017). Dadiannao: a neural network supercomputer. *IEEE Transactions on Computers*, *66*(1), 73–88. ISSN 0018-9340. https://doi.org/10.1109/TC.2016.2574353.

Maass, W. (2000). On the computational power of winner-take-all. *Neural Computation*, *12*(11), 2519–2535.

Manes, F., Sahakian, B., Clark, L., Rogers, R., Antoun, N., Aitken, M., Robbins, T. (2002). Decision-making processes following damage to the prefrontal cortex. *Brain: A Journal of Neurology*, *125*(Pt 3), 624–639.

Mao, Z.H., & Massaquoi, S.G. (2007). *IEEE Transactions on Neural Networks*, *18*(1), 55–69.

Markov, N.T., Ercsey-Ravasz, M., Van Essen, D.C., Knoblauch, K., Toroczkai, Z., Kennedy, H. (2013). Cortical high-density counterstream architectures. *Science*, *342*(6158), 1238406.

Markram, H., Lubke, J., Frotscher, M., Roth, A., Sakmann, B. (1997). Physiology and anatomy of synaptic connections between thick tufted pyramidal neurones in the developing rat neocortex. *Journal of Physiology*, *500*(Pt 2), 409–440. ISSN 0022-3751 (Print); 0022-3751 (Linking).

Marreiros, A.C., Daunizeau, J., Kiebel, S.J., Friston, K.J. (2008). Population dynamics: variance and the sigmoid activation function. *NeuroImage*, *42*(1), 147–157.

Mason, A., & Larkman, A. (1990). Correlations between morphology and electrophysiology of pyramidal neurons in slices of rat visual cortex. II. Electrophysiology. *The Journal of Neuroscience*, *10*(5), 1415–1428.

Mason, A., Nicoll, A., Stratford, K. (1991). Synaptic transmission between individual pyramidal neurons of the rat visual cortex *in vitro*. *Journal of Neuroscience*, *11*(1), 72–84.

McKinstry, J.L., Fleischer, J.G., Chen, Y., Gall, W.E., Edelman, G.M. (2016). Imagery may arise from associations formed through sensory experience: a network of spiking neurons controlling a robot learns visual sequences in order to perform a mental rotation task. *PLos ONE*, *11*(9), e0162155.

Melin, J. (2005). Does distribution theory contain means for extending poincaré–bendixson theory? *Journal of Mathematical Analysis and Applications*, *303*(1), 81–89. ISSN 0022-247X. https://doi.org/10.1016/j.jmaa.2004.06.069.

Miller, P., & Katz, D.B. (2013). Accuracy and response-time distributions for decision-making: linear perfect integrators versus nonlinear attractor-based neural circuits. *Journal of Computational Neuroscience*, *35*(3), 261–294.

Munakata, Y., Herd, S.A., Chatham, C.H., Depue, B.E., Banich, M.T., O'Reilly, R.C. (2011). A unified framework for inhibitory control. *Trends in Cognitive Sciences (Regul. Ed.)*, *15*(10), 453–459.

Patel, M., & Rangan, A. (2017). Role of the locus coeruleus in the emergence of power law wake bouts in a model of the brainstem sleep-wake system through early infancy. *Journal of Theoretical Biology*, *426*, 82–95.

Perin, R., Berger, T.K., Markram, H. (2011). A synaptic organizing principle for cortical neuronal groups. *Proceedings of the National Academy of Sciences of the USA*, *108*(13), 5419–5424.

Platt, M.L., & Glimcher, P.W. (1999). Neural correlates of decision variables in parietal cortex. *Nature*, *400*(6741), 233–238.

Polsky, A., Mel, B.W., Schiller, J. (2004). Computational subunits in thin dendrites of pyramidal cells. *Nature Neuroscience*, *7*(6), 621–627.

Ratcliff, R. (1978). A theory of memory retrieval. *Psychological Review*, *85*(2), 59–108.

Ratcliff, R., Smith, P.L., Brown, S.D., McKoon, G. (2016). Diffusion decision model current issues and history. *Trends in Cognitive Sciences (Regul. Ed.)*, *20*(4), 260–281.

Rauch, A., La Camera, G., Luscher, H.R., Senn, W., Fusi, S. (2003). Neocortical pyramidal cells respond as integrate-and-fire neurons to *in vivo*-like input currents. *Journal of Neurophysiology*, *90*(3), 1598–1612. ISSN 0022-3077 (Print); 0022-3077 (Linking). https://doi.org/10.1152/jn.00293.2003.

Roxin, A., Riecke, H., Solla, S.A. (2004). Self-sustained activity in a small-world network of excitable neurons. *Physical Review Letters*, *92*, 198101. https://doi.org/10.1103/PhysRevLett.92.198101.

Rutishauser, U., Douglas, R.J., Slotine, J.J. (2011). Collective stability of networks of winner-take-all circuits. *Neural Computation*, *23*(3), 735–773.

Sachdev, P.S., & Malhi, G.S. (2005). Obsessive-compulsive behaviour: a disorder of decision-making. *The Australian and New Zealand Journal of Psychiatry*, *39*(9), 757–763.

Schall, J.D. (2001). Neural basis of deciding, choosing and acting. *Nature Reviews. Neuroscience*, *2*(1), 33–42.

Shadlen, M.N., & Newsome, W.T. (2001). Neural basis of a perceptual decision in the parietal cortex (area LI,P) of the rhesus monkey. *Journal of Neurophysiology*, *86*(4), 1916–1936.

Shpiro, A., Curtu, R., Rinzel, J., Rubin, N. (2007). Dynamical characteristics common to neuronal competition models. *Journal of Neurophysiology*, *97*(1), 462–473.

Sporns, O., & Honey, C.J. (2006). Small worlds inside big brains. *Proceedings of the National Academy of Sciences of the USA*, *103*(51), 19219–19220. ISSN 0027-8424 (Print); 0027-8424 (Linking). https://doi.org/10.1073/pnas.0609523103.

Taube, J.S. (2007). The head direction signal: origins and sensory-motor integration. *Annual Review of Neuroscience*, *30*, 181–207.

Thomas, N.W., & Pare, M. (2007). Temporal processing of saccade targets in parietal cortex area LI,P during visual search. *Journal of Neurophysiology*, *97*(1), 942–947.

Usher, M., & McClelland, J.L. (2001). The time course of perceptual choice: the leaky, competing accumulator model. *Psychological Review*, *108*(3), 550–592.

van den Heuvel, M.P., Stam, C.J., Boersma, M., Hulshoff Pol, H.E. (2008). Small-world and scale-free organization of voxel-based resting-state functional connectivity in the human brain. *Neuroimage*, *43*(3), 528–539. ISSN 1095-9572 (Electronic); 1053-8119 (Linking). https://doi.org/10.1016/j.neuroimage.2008.08.010.

Wang, X.J. (2002). Probabilistic decision making by slow reverberation in cortical circuits. *Neuron*, *36*(5), 955–968.

Watts, D.J., & Strogatz, S.H. (1998). Collective dynamics of 'small-world' networks. *Nature*, *393*(6684), 440–442. ISSN 0028-0836 (Print); 0028-0836 (Linking). https://doi.org/10.1038/30918.

Wei, W., & Wang, X.J. (2016). Inhibitory control in the cortico-basal ganglia-thalamocortical loop complex regulation and interplay with memory and decision processes. *Neuron*, *92*(5), 1093–1105.

Wilson, H.R., & Cowan, J.D. (1972). Excitatory and inhibitory interactions in localized populations of model neurons. *Biophysical Journal*, *12*, 1–24.

Xie, X., Hahnloser, R., Seung, S.H. (2002). Double-ring network model of the head-direction system. *Physical Review E*, *66*(4), 041902.

Yamada, W., Koch, C., Adams, P. (1989). Multiple channels and calcium dynamics. In *Methods in neuronal modeling: from synapses to networks* (pp. 97–133). Cambridge: MIT Press.

You, H., & Wang, D. (2017). Neuromorphic implementation of attractor dynamics in a two-variable winner-take-all circuit with nmdars: A simulation study. *Frontiers in Neuroscience*, *11*, 40. ISSN 1662-453X. https://doi.org/10.3389/fnins.2017.00040.